ALMA MATER STUDIORUM
UNIVERSITA' DI BOLOGNA
SCUOLA DI SCIENZE

Corso di laurea magistrale in Biologia Marina

Prokaryotic community structure in ultra-slow spreading Southwest Indian Ridge

Tesi di laurea in

Microbiologia Marina e Cicli Biogeochimici

Relatore
Prof. Roberto Borghese

Presentata da
Gilda Varliero

Correlatore
Massimiliano Molari

II sessione
Anno Accademico 2014/2015

Contents

1. Introduction

1.1 Deep sea ecosystems

Deep-sea ecosystem extends from the continental shelf, about 200 m depth, to the abyssal environments, of which the deepest point is the Mariana Trench (11000 m; Danovaro et al., 2014). This ecosystem includes about 95% of seafloor and about 67% of the Earth's lithosphere (Jørgensen and Boetius et al., 2007). Here, the average depth is about 4000 m, the average temperature is below than 4 °C and the average hydrostatic pressure is about 400 atm (Danovaro et al., 2014). Sunlight penetrates maximum up to 300 m of the water column, so the deep sea is in the dark and no photosynthesis occurs here (Orcutt et al., 2011), and therefore the dominant biological process is respiration. About 1-40% of the photosynthetic fixed carbon in the euphotic zone is exported in dark deep sea (Herndl et al., 2013), but only 0,4% of primary production is buried in oceanic sediment, due to efficiently removal of organic matter by pelagic heterotrophic microorganisms (Middelburg et al., 2007). For all these characteristics, this environment was considered homogenous and extreme for life. However in the last fifty years, the intensification of explorations and the development of technology in remote mapping (e.g. multibeam acoustics) and observation (e.g. videos from remotely or autonomous operated vehicles) revealed a broad range of benthic deep sea habitats, which provide highly diverse condition for metazoan and microbial communities favouring high biodiversity. In particular our view of deep-sea changed drastically with the discovery of hydrothermal vents and their associated fauna along the Galapagos Rift in 1977 (Corliss et al., 1979) and of cold seeps in the 1980s on continental margins (Paull et al., 1985).

1.2 Hydrothermal systems and life

In seabed systems where hydrothermal circulation is present, life thrives. Here, the primary producers are chemolithoautotrophics, microorganisms able to use chemical compounds as energy source to produce biomass fixing carbon dioxide into organic compounds (McCollom and Shock, 1997). This process is called chemosynthesis. The high abundance and intense activity of chemolithotrophs make veritable “oasis of food” in the deep-sea (Tunnicliffe, 1988). Indigenous organic matter allows the presence of rich communities of metazoan like tube warms, clams, mussels and shrimps. They are supported by primary production in different ways: symbiotic associations, direct consumption of microbes or parasitism. These macrofaunal communities are endemic and general ephemeral because depend totally on microbial productivity generated by hydrothermal vent discharge (Kelley et al., 2002).

Seafloor hydrothermal circulation plays a significant role in the cycling of energy and mass between the solid earth and the oceans. Hydrothermal vent is a zone of the oceanic crust where geothermal heated water leaks. The mechanism is a rapidly advective fluid flow. Deep seawater percolates downward into exposed outcrops of the ocean´s crust due to thermal and pressure gradients; it is first heated and then undergoes chemical modification through reaction with the host rocks as it continues downward reaching maximum temperatures which can exceed 400°C. At these temperatures the fluid become buoyant and rise back to the seafloor where they are expelled into the overlaying water column (German and Seyfried, 2014). When the thermal gradient is strong, there is formation of hydrothermal mineral deposits in the form of chimney structures, called black smokers. Black smokers are an example of seafloor hydrothermal circulation in

high temperature (>400 °C) but they are a small fraction of the total hydrothermal heat flux close to the ridge axes. Every different hydrothermal vent has a different composition and varies on short timescale. Chemistry of vent fluids is largely dependent on the composition of the source rock, temperature and pressure condition that found during the transition in the ocean crust (Kelley et al., 2002). In these systems, chemolithoautotrophic community thrives because there is an input of water rich in reduced inorganic compounds like hydrogen, carbonic dioxide, methane, reduce sulfur compounds, iron, manganese and ammonium. Furthermore, metabolic pathways and their efficiencies are influenced by which kind of electron acceptors are present in the system: oxygen, nitrate, nitrite, manganese and iron oxides, oxidized sulfur compounds, carbon dioxide (Orcutt et al., 2011). In the dark ocean, metabolic strategies are based on chemical redox reactions, which occur when they are thermodynamically favorable and yield enough energy for ATP generation. The hydrothermal vents (Figure 1.1), due to wide range and high amount of reduced and oxidized are characterized by high biomass of prokaryotes and high metabolic diversity compounds (Whitman et al., 1998; DeLong, 2004).

1.3 Ridge Systems

After the discovery of the fist submarine hydrothermal vent, many hydrothermal vents have been discovered and more than 60% are distributed along mid-ocean ridge (Tao et al. 2011). The mid-ocean ridge is a continuous chain of underwater mountains and volcanoes that is spread around the Earth. This global spreading system occurs where there is the boundary of two tectonic plates (Figure 1.2) and extends over 60000 km on the oceanic crust and represents the main region of

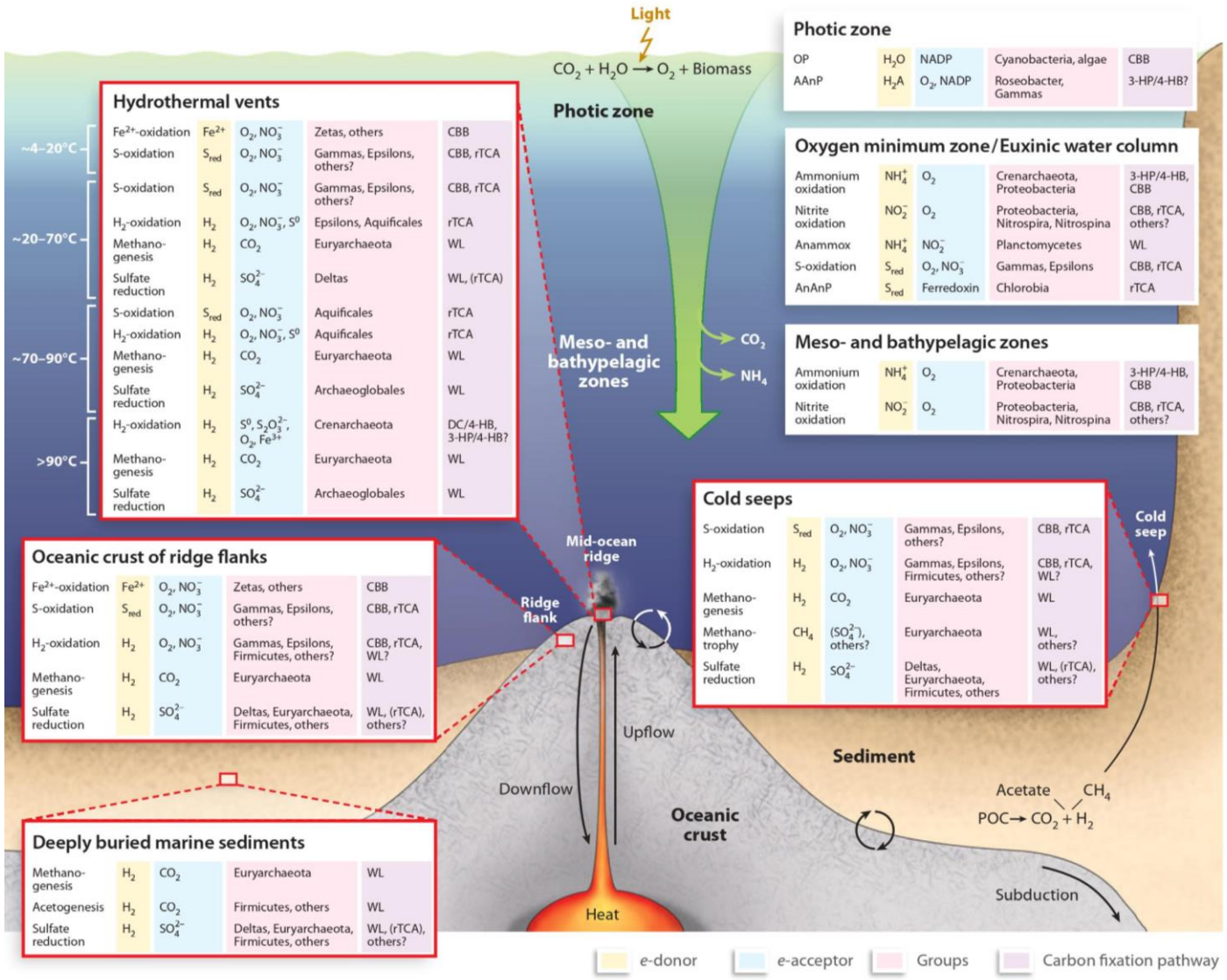

Figure 1.1. Metabolisms of autotrophs, electron donor and acceptor compounds and carbon fixation pathways in different ocean systems. Relevant carbon fixation pathways, apart from the Calvin-Benson-Bassham cycle (CBB), the reductive tricarboxylic acid cycle (rTCA), the Wood-Ljungdahl pathway (WL), the 3-hydroxypropionate/4-hydroxybutyrate cycle (3-HP/4-HB), and the dicarboxylate/ 4-hydroxybutyrate cycle (DC/4-HB). Recently, it became clear that these pathways provide important contributions to carbon fixation in many oceanic environments, most notably deep-sea hydrothermal vents, cold seeps, the meso- and bathypelagic ocean, oxygen deficiency zones, redoxclines, and euxinic waters. Abbreviations: AnAP, anoxygenic aerobic photosynthesis; OP, oxygenic photosynthesis; anammox, anaerobic ammonium oxidation; S-oxidation, sulphur oxidation; Fe2+-oxidation, iron oxidation; Sred, reduced sulphur compounds; Gammas, Gammaproteobacteria; Epsilons, Epsilonproteobacteria; Zetas, Zetaproteobacteria; POC, particulate organic carbon. (Hugler and Sievert, 2011)

internal heat transport and dissipation of Earth, hosting almost 70% of Earth´s magmatism (Standish et al. 2010). Different morphology of spreading ridge can develop based on different factors such the melt supply rate, the spreading rate and the effectiveness of hydrothermal cooling (Kelley et al. 2002). The main classification of the spreading ridge is based on the spreading rate (Figure 1.2): 1) fast spreading ridges have a spreading rate between 80-180 mm/yr; this system is characterized by low axial highs of about 400 m and well-defined axial valleys at the ridge center; the axial topography is strongly correlated with the spreading rate. Their morphology tends to be dominated by volcanism. 2) Intermediate spreading ridges has a spreading rate between 55-77 mm/yr and they have long alternating sections with either slow or fast spreading ridge morphology. 3) Slow spreading ridges have a spreading rate of less than 55 mm/yr. The rift valley is deep with highly variable and steep relieves from 400 to

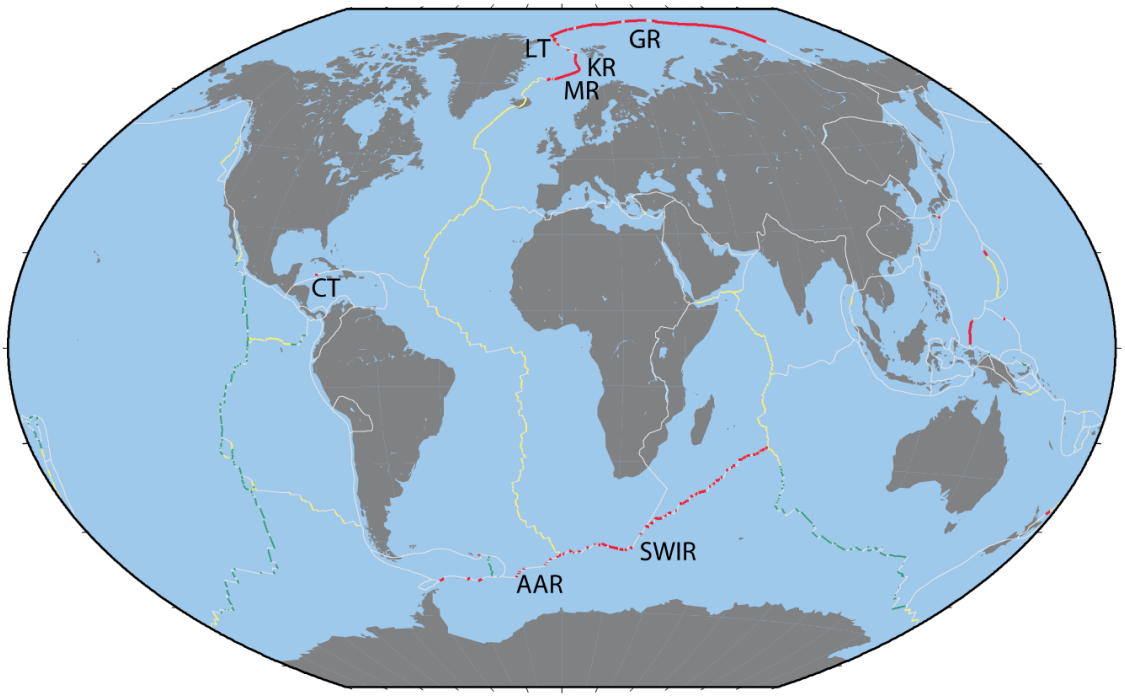

Figure 1.2. . The global ridge system. In grey are the global plate boundaries; in green the fast spreading ridges (spreading rate of 80-100 mm/yr); in red the ultraslow spreading ridges (spreading rate lower than 20 mm/yr); and in yellow all the other ridge segments. GR = Gakkel ridge, IT = lena trough, KR = Knipovich ridge, MR = Mohns ridge, CT = Cayman trough, AAR = America-Antarctic ridge, and SWIR = Southwest Indian ridge. (Snow and Edmonds, 2007)

2500 m and rough rift mountain topography weakly correlated to spreading rate. The morphology tends to be dominated by tectonic force (Dick et al. 2003). 4) Ultraslow spreading ridges.

Ultraslow spreading ridges include the Southwest Indian Ridge, the Gakkel Ridge and several smaller ridges. They are mainly sited at the poles with a total length of 15000 km, representing about 25% of the global mid ocean ridge system (Solomon, 1989). This ridge class is characterized by spreading rate of <20 mm/year and a thin oceanic crust (1-4 km) (Snow and Edmonds, 2007). The morphology of this ridge is similar of that of slow spreading ridge: high valley walls and rugged rift mountains. The axis of ultraslow spreading ridge is constituted by both magmatic and amagmatic accretionary ridge segments and they are linked together to make up a “supersegment”. In faster systems there are mainly magmatic segments that are linked together between transform faults to build first-order segments. In these systems transform faults are not present and are replaced by amagmatic accretionary ridge segments that are key component of ultraslow spreading ridges. Contrary to magmatic segments, they can assume any orientation relative to the spreading direction (Dick et al. 2003).

Extensive outcrops of serpentinized peridotites are exposed in the crust of these systems (Cannat et al., 2010), due to prevalence of tectonic processes that lead the uplift and exposure of material from upper mantle and lower crust. This material, low-silica ultramafic rocks (mainly olivine and pyroxene), undergoes water-rock reactions (Schrenk et al., 2013). The result is the oxidation of ferrous iron from olivine and pyroxene, the precipitation of ferric iron in magnetite and other minerals and the release of diatomic hydrogen. The combination of diatomic hydrogen and carbon dioxide or carbon oxide under highly reducing conditions

leads to formation of methane (Charlou et al., 2010). These reactions are highly exothermic and contribute significantly to the overall hydrothermal fluxes (Früh-Green et al. 2003). These fluxes provide reduced energy to the system and develop a diffused dissipation of the heat from the lithosphere (Dick et al. 2003). Another factor that could lead to a heat diffused system is the low thickness of the crust, due to the proximity of hot mantle to seawater and sediments. All these aspects could have a strong impact on generation of hydrothermal circulation and therefore on the structure of the microbial community, whose structure could be influenced (e.g. less chemolithotrophs) if a minor input of reduced molecules occurs as result of diffused input of hydrothermal fluids (Kelley et al., 2007).

Habitats that have characteristics similar to ultramafic systems are seep systems. Here the leakage of heat is widespread like in ultramafic systems and the fluid have a similar composition, being rich in methane and poor of reduced metals (Hovland et al., 2012).

In 1990s a linear relationship between the spreading rate and hydrothermal activities was proposed (Baker et al., 1996). Because of the very slow spreading rate of these ridges they were supposed to be inactive and without any hydrothermal activity. Furthermore, their geographical position (mainly the poles) didn't allow the study of this class of ridge until a development of research devices (German et al., 2010). Afterwards, the ultraslow spreading ridge was supposed to have only tectonic activities because the magma supply was supposed to be insufficient to support significant convection (Edmonds, 2010). First indirect evidence of the presence of hydrothermal venting in ultraslow spreading ridges was obtained in 1997 through a survey of water anomalies in SWIR (German et al., 1998). The first hydrothermal plume was detected during at the R/V Knorr

Cruise 162 in segment 10 and 16°E of SWIR (Bach et al., 2002). Another evidence of hydrothermal activity in this system was obtained in 2007 during the Chinese research cruise DY115-19 (Tao et al., 2012). At the Gakkel Ridge, evidences of hydrothermal activity where found in 2003 during the AMORE cruise, and in 2008 during an International Polar Year expedition pyroclastic deposits with fragmented magma were found (Sohn et al., 2008). All these works support the hypothesis that high temperature hydrothermal circulation is widespread along all ultraslow spreading ridges despite the low magma supply.

1.4 South West Indian Ridge

Southwest Indian Ridge (SWIR) extends between the Rodrigues Triple Point in the southern Indian Ocean and the Bouvet Triple Junction in the south Atlantic, so it represents the only way for chemosynthetic deep sea vent fauna for their dispersion between Atlantic and Pacific ridge systems (Baker at al., 2004). The vent fields may provide suitable “stepping stone” niche environments that can sustain chemosynthetic ecosystems and enhance the flow among different systems. During the ChEss programme, whose aim was an improving of the knowledge of the biogeography of deep water chemosynthetically driven systems, it was observed as vent species along the Southeast Indian Ridge showed increasing influence of Pacific faunas, whereas along the Southwest Indian Ridge, Atlantic influences were greater (Tyler et al., 2003). However, due to few studies describing the hydrothermal communities at SWIR (Peng et al, 2011), there are weak evidences in support of this observation.

The SWIR can be divided into a number of subsections based on changes in the obliquity of the ridge axis and on the variation of regional axial depth. As obliquity increase, the spreading rate slows proportionally (Tao et al., 2012). The average

speed of SWIR is almost 14 mm/year but we can find several segments with different speed; in the work of Dick et al. (2003) this ridge is defined as a transitional system between slow and ultraslow spreading ridge.

The SWIR segment, which I deal in my thesis, extends between 10°-16°E. The average depth is 4000 m and extended peridotite outcrops in the ridge axis are present. This area has the slowest spreading rate of any other oceanic ridge (8.4 mm/year); this peculiar characteristic is due to its very oblique orientation (51° from the spreading direction; Dick et al., 2003). Here, during the R/V *Knorr* Cruise 162, evidences of two active vent sites, massive sulfide deposits, sepiolite deposits, silica deposits and Mn-oxide breccias were revealed. This discovery is remarkable because it proves that the presence of hydrothermal material and activity is not strictly connected with magma supply rate and mantle upwelling, as along this section they are lower than on any other studied ridge segments. Therefore, the presence of hydrothermal activity in this area could reflect a tectonic control on fluid circulation (Bach at al., 2002), and contribute to dispersion route for the hydrothermal fauna.

2. Objectives

In 2013 along the segment 10°-16° E of the South West Indian Ridge a multidisciplinary survey, involving seismologic, geologic, microbiological analyses, was carried out during the expedition ANTXXIX/8.

Sediment sampling was focused on selected target sites that were characterized by anomalies in water column, situated in fault systems or showed high heat flux. No hydrothermal plumes or black smoker systems were found in this area. However, high heat flux was measured in one station, and in another station sediment enriched in reduced compounds was collected and the presence of vent fauna were reported by photographic survey. All these aspects suggest that a hydrothermal circulation was present in this investigated SWIR segment. Thus if this hydrothermalism is associated to fluid emissions then benthic organisms should be influenced in some extent.

The aim of my work is to provide a biological evidence of the presence of hydrothermal circulation in this area, as no previous microbial studies have been conducted in this segment. In my study, I hypothesized that a difference in the microbial community structure is present amongst areas that show different geochemical characteristics and in particular, I expect to find a microbial community related to those isolated from hydrothermal-driven systems in the area where high reduced molecules and hydrothermal fauna have been observed.

3. Materials and Methods

3.1 Sample collection

The samples were collected during the expedition ANTXXIX/8 between November and December 2013 in the segment 10°-16°E of the Southwest Indian Ridge (SWIR), with R/V POLARSTERN. Sediment samples have been taken from seabed at depth range of 2228 and 4869 m. Superficial sediment samples, the first 30-40 cm, have been collected with multi corers device (MUC) and subsurface samples, from 1 m below seafloor (bsf) up to 6 m bsf, with a gravity core (GC). All sampled sediments were stored at -80° C. I investigated sediments sampled in one reference station, located outside and south of the rift valley, and 5 stations inside the valley (Figure 3.1). I analysed one sediment layer, 0-5 cm bsf, in the reference area and three different layers in areas situated inside the ridge valley: 0-5 cm, 110 cm and 410 cm bsf (Table 3.1). These layers have been selected according to geochemical profiles (Figure 3.2).

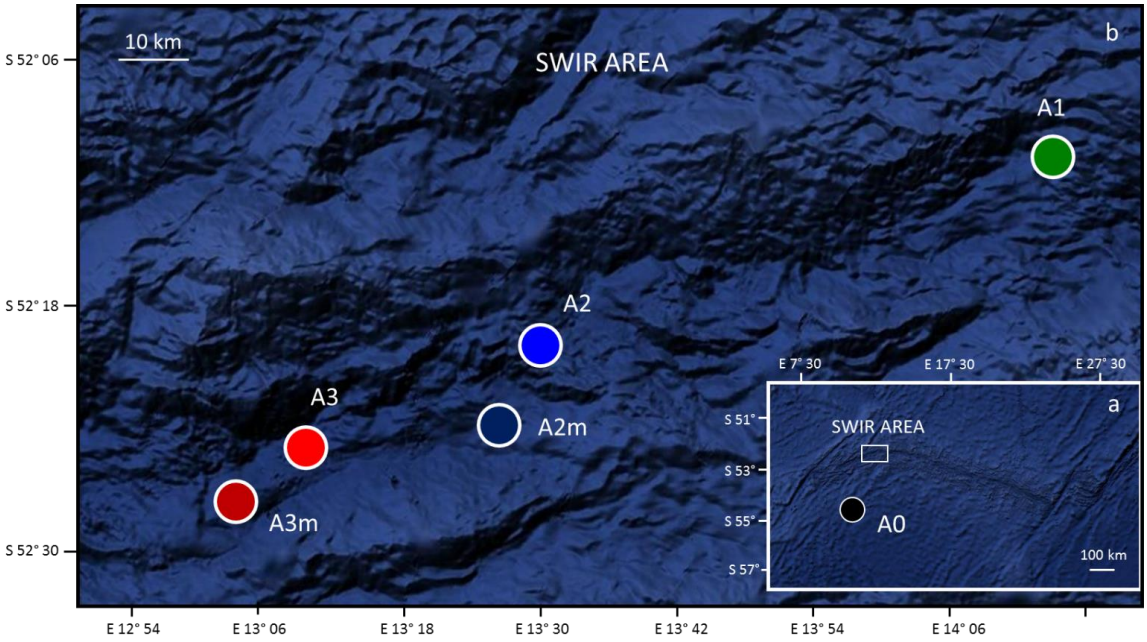

Figure 3.1. Map of study areas; a) SWIR area and the reference station (A0); b) the location of the study stations inside the SWIR area.

Station	Depth bsf cm	Area	Sampling Station	Device	Latitude	Longitutide	Water Depth m	Temperature °C	Area Characteristic
A0	0-5	A0	PS81/626	TV-MUC	-54°55.547'	12°27.748'	4869		Reference Area (South Mount)
A1	0-5	A1	PS81/649	TV-MUC	-52°10.095	14°10.620'	3655		High Heat Flow Area
A2	0-5	A2	PS81/659	TV-MUC	-52°22.051'	13°19.215'	3941		Heat Flow Area (Bach et al.,2002)
A2m	0-5	A2	PS81/639	TV-MUC	-52°26.063'	13°18.287	4375		Heat Flow Area (Bach et al.,2002)
A3	0-5	A3	PS81/661	TV-MUC	-52°26.462'	13°8.196'	4415		Axis Centre
A3m	0-5	A3	PS81/636	TV-MUC	-52°29.790'	13°3.870'	4199		Clam Area
A1	110	A1	PS81/653	gravity core	-52°10.220'	14°10.830'	3709	2.3	High Heat Flow Area
A2	110	A2	PS81/656	gravity core	-52°21.970'	13°19.040'	3968	1.0	Heat Flow Area (Bach et al.,2002)
A3	110	A3	PS81/657	gravity core	-52°26.450'	13°8.110'	2228	0.5	Axis Centre
A1	410	A1	PS81/653	gravity core	-52°10.220'	14°10.830'	3709	5.8	High Heat Flow Area
A2	410	A2	PS81/656	gravity core	-52°21.970'	13°19.040'	3968	1.5	Heat Flow Area (Bach et al.,2002)
A3	410	A3	PS81/657	gravity core	-52°26.450'	13°8.110'	2228	0.8	Axis Centre

Table 3.1. Description of stations here investigated.

3.2 Area Characterisation

During RV POLARSTERN cruise P81 to the SWIR, an integrated study was carried out employing seismology, geology, microbiology, deep-sea ecology, heat flow and others. The objectives of this expedition were to confirm the presence of hydrothermal circulation, hypothesized by earlier study (Bach et al., 2002), and to identify and localize the origin of hydrothermal plume.

The data collected on field did not provide evidence of temperature, redox potential and turbidity anomalies in water column, usually applied like a proxy for hydrothermal plume signature, as previously described by Bach and colleagues (2002), as well as vigorous fluid flow in the form of black smokers or shimmering water could not be observed at seafloor. However enhanced heat flow due to upward pore water migration was measured. This leads to values of very high heat flow (up to 850 mW/m^2) and advection rates up to 25 cm/s. Enhanced biomass and a greater variation of megafauna along those sites of high heat flow could be inferred from reconnaissance observations with a camera sledge. A closer investigation of microbial activity in the material of gravity corers revealed favorable living conditions for microorganisms. Furthermore in few stations chemosynthetic fauna, typical of deep-sea hydrothermal habitats such as clams and worms, has been collected.

The geochemical analysis of pore water extracted both from MUC and GC sediments showed interesting differences between stations inside the valley and the reference station. In particular anomalies and upward decreasing in concentration of ammonia, methane, sulfide and dissolved inorganic carbon (DIC) suggest the presence of hydrothermal emissions in western area of SWIR's segment investigated (Figure 3.2).

According with these preliminary results the sampling stations were grouped into four areas with different characteristics: 1) area 0 (A0): reference station located outside and south of SWIR; 2) area 1 (A1): higher heat flow; 3) area 2 (A2): sites were plume signature were reported in previous study; 4) area 3 (A3): sites with geochemical anomalies in pore water and where chemosynthetic fauna (e.g. Vesycomid clam) has been retrieved.

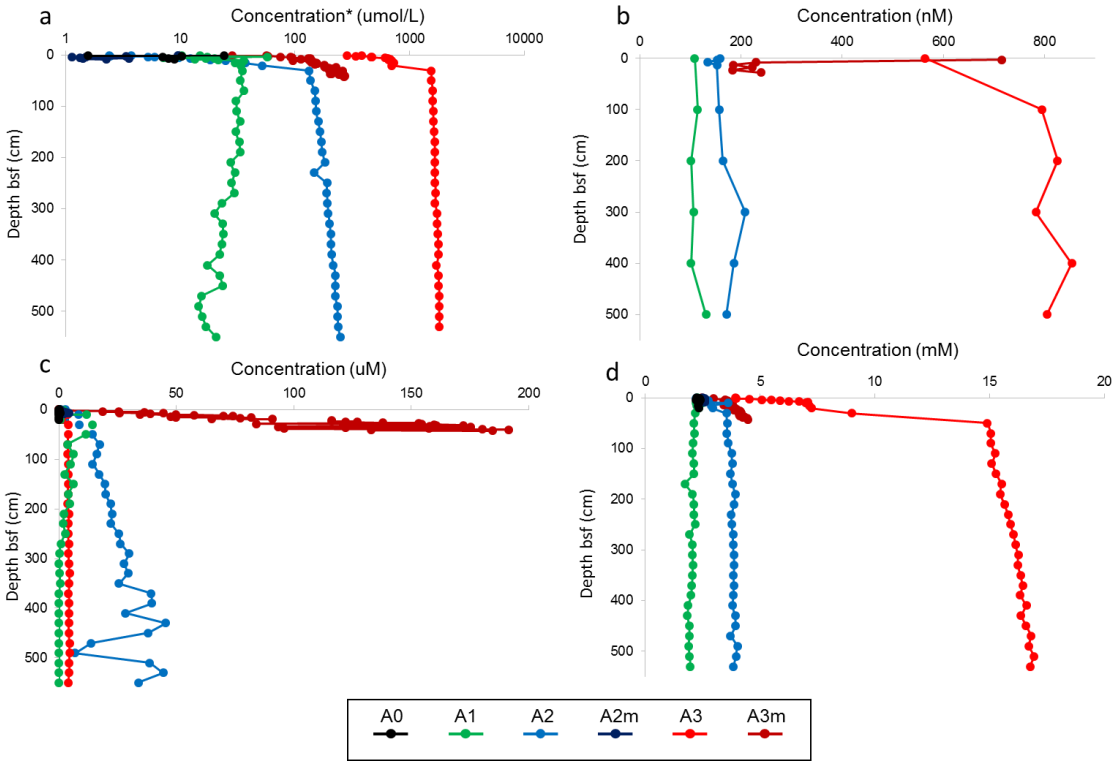

Figure 3.2. Geochemical sedimentary profiles for MUC and gravity core samples: a) Ammonium; b) Methane; c) Sulphide; d) DIC. * Logarithmic scale.

3.3 DNA Extraction

In order to study the microbial community, DNA was extracted from different stations and layers of the four areas described above. I selected 6 samples of the layer 0-1 cm, 6 samples of the layer 1-5 cm, 4 samples of 110 cm and 4 samples of 410 cm (shown in Table S1). As the samples are constituted by different sediment typologies, and this can affect DNA extraction yield, I tested different extraction procedures in order to obtain similar DNA amount and quality from all areas. The following DNA extraction kits were tested: UltraClean™ Soil DNA Isolation Kit (MoBio laboratories Inc.), FastDNA™ SPIN Kit for Soil (Q-BIOgene), PowerSoil™ DNA Isolation Kit (MoBio laboratories Inc.). All the extractions were performed following the manual protocols. I selected four different samples according with sediment tipology: A0, A2, A3 and one subsurface sample (soil characteristics shown in Table 3.2). I extracted DNA from 0.5 g of sediment from each sample. After each extraction, DNA concentrations and DNA quality, measured as 260/280 (it indicates the purity of DNA and RNA; a ratio of about 1.8 indicates “pure” DNA) and 260/230 ratio (it indicates the nucleic acid purity; the ratio is normally in the range of 2.0-2.2), have been quantified with NanoDrop (Thermo SCIENTIFIC 1000). As shown in Table 3.2, the higher amount of DNA was obtained with FastDNA™ SPIN Kit for Soil but with this method, the lower quality of DNA was obtained. This could be due to presence of humic acids in the sediments (Tebbe and Vahjen, 1993); in order to remove these compounds, I performed a DNA precipitation on samples extracted with FastDNA™ SPIN Kit for Soil (Table 3.2). Precipitation was executed in ethyl acetate and isopropanol. After the addition of an amount of ethyl acetate (7.5 M) equal to 1/3 of the sample volume and of an amount of isopropanol equal to the volume of the sample, DNA

Sample	Soil characteristic	DNA amount ng	260/280	260/230
$A0_{UC}$	Compact surface sediment	0.2	1.89	0.96
$A0_{PS}$	Compact surface sediment	0.7	1.73	1.59
$A0_{F}$	Compact surface sediment	2.7	2.04	0.05
$A0_{P}$	Compact surface sediment	0.7	1.68	1.02
$A2_{UC}$	Soft surface sediment	0.9	1.90	1.66
$A2_{PS}$	Soft surface sediment	0.0	1.83	0.99
$A2_{F}$	Soft surface sediment	1.8	2.31	0.04
$A2_{P}$	Soft surface sediment	0.4	1.79	1.93
$A3_{UC}$	Fluffy sediment (diatom ooze)	0.1	1.94	1.76
$A3_{PS}$	Fluffy sediment (diatom ooze)	0.0	2.54	1.07
$A3_{F}$	Fluffy sediment (diatom ooze)	0.5	3.81	0.01
$A3_{P}$	Fluffy sediment (diatom ooze)	0.1	2.27	0.76
Sub_{PS}	Compact subsurface sediment	0.0	4.59	0.45
Sub_{F}	Compact subsurface sediment	0.7	2.81	0.01
Sub_{P}	Compact subsurface sediment	0,1	1.46	0.56

Table 3.2. Results of DNA extractions carried out with different extraction kits. UC, samples extracted with the UltraClean™ Soil DNA Isolation Kit; F, FastDNA™ SPIN Kit for Soil; PS, PowerSoil™ DNA Isolation Kit; P, FastDNA™ SPIN Kit for Soil followed by precipitation. Sub, subsurface sample. 260/280 and 260/230 are ratios that indicate the purity of the DNA: a 260/280 ratio of about 1.8 indicates “pure” DNA and 260/230 ratio indicates a good nucleic acid purity if it is in the range of 2.0-2.2.

was incubated overnight at -20 °C. Then a centrifugation was performed to allow the DNA precipitation and the removal of the supernatant. DNA was suspended in ethanol 70% in order to clean again the DNA. The solution was centrifuged again and the ethanol was removed. The last suspension was made with TE buffer. All the DNA samples were stored at -20°C.

Furthermore, I tested the amplificabily of the 16S segment of the extracted DNA, performing a PCR (Polymerase Chain Reaction). The amplifications were carried out in 20-µl reaction mixtures that consisted of 1 µl of DNA template, 1.5 mM 10× PCR buffer (Mg++), 200 µM deoxynucleoside triphosphate, 0.5 µM concentrations of each primer, 0.0125 U/µl of *Taq* DNA polymerase. In order to amplify nearly full length 16S rRNA, I used universal bacterial primers GM3F and GM4R (5'-AGAGTTTGATCMTGGC-3' and 5'-TACCTTGTTACGACTT-3'); and archaeal universal primers 20F (5‘-TTCCGGTTGATCCYGCCRG-3‘) and 1492R (5'-TACGGYTACCTTGTTACGACTT-3‘). 20 ul of DNA from each sample was

loaded in Thermal Cycler (ThermoFisher SCIENTIFIC): bacterial DNA was amplified for 30 cycles (1 min of denaturation at 95°C, 1.5 min of annealing at 44°C, and 3 min of elongation at 72°C); archaeal DNA was amplified for 30 cycles (1 min of denaturation at 95°C, 1 min of annealing at 55°C, and 2 min of elongation at 72°C). The electrophoresis was performed on agarose gel (1%); in order to control the reliability of PCR, positive and negative controls were used. The gel was visualized under ultraviolet light after ethidium bromide bath. In Figure 3.3, it is shown as the better results were obtained with FastDNA^{TM} SPIN Kit for Soil.

FastDNA^{TM} SPIN Kit for Soil was selected to extract DNA from all the samples reported in the Table S1. The FastDNA extraction is not a chloroform phenol method; briefly the procedure followed these steps: i) the mechanical cell lysis is carried out by a mixture of ceramic and silica particles; ii) the addition of reagents permits to protect and solubilize nucleic acid upon cell lysis, minimize RNA contaminations, enhance the protein precipitation; iii) the addition of a DNA binding reagent allows the DNA holding; iv) the passage of DNA through a filter permits the holding of DNA at the filter (this passage has to be repeated 3-4 times); v) the DNA is eluted in pure PCR water and stored at -20°C. After every DNA extraction, DNA yield was measured.

The DNA concentrations of subsurface samples were lower than the surface sediment (Table S1), thus the subsurface DNA was precipitated and suspended in appropriate volume to have comparable concentration with surficial DNA (precipitation procedure is described above). Furthermore, in order to have comparable amount of DNA, I performed 2 extractions on surface samples and 4

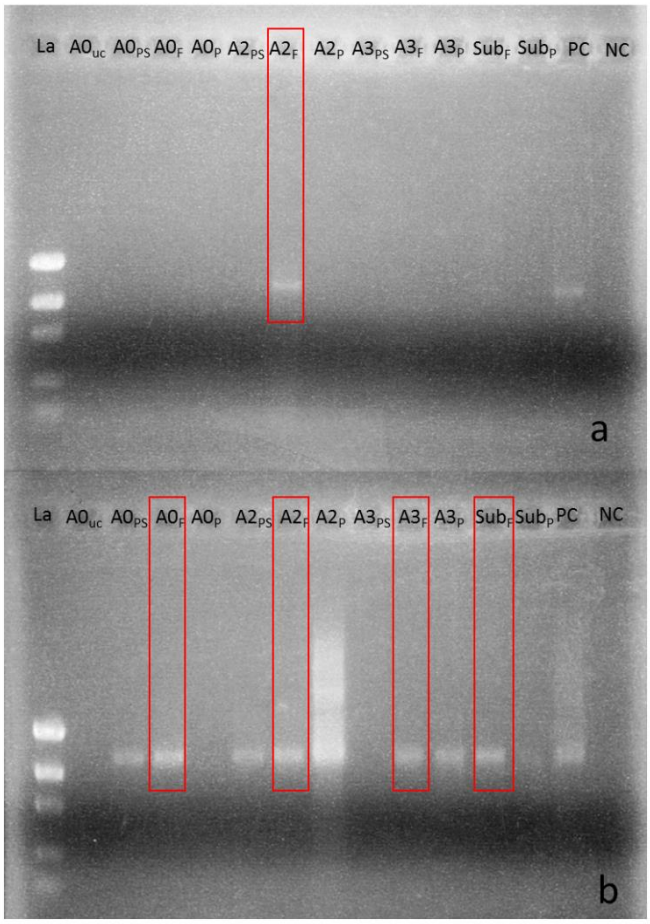

Figure 3.3. Electrophoretic run in agarose gel (1%) for PCR products (amplified 16S segments) of DNA extracted with different kits; a)archaeal 16S; b)bacterial 16S. Highlighted in red are the DNA samples extracted with FastDNA^{TM} SPIN Kit for Soil.

extractions on subsurface samples. The DNA extracted from layers 0-1 cm and 1-5 cm was combined. A total of 2 g of sediment per samples were extracted from both surface and subsurface layers.

To verify that the extracted DNA was amplifiable, I performed PCR on all the extracted DNA samples (with the same procedure described above). I had some problems to amplify archaeal DNA, which were resolved changing annealing temperature, PCR reaction mixture and using a pair of primers that amplify a shorter fragment (958R [5'-CCGGCGTTGANTCCAATT-3'] and 20F).

In the Table 3.3, the selected and shipped samples are shown; the Figure 3.4 shows PCR products on electrophoresis gel of these final samples.

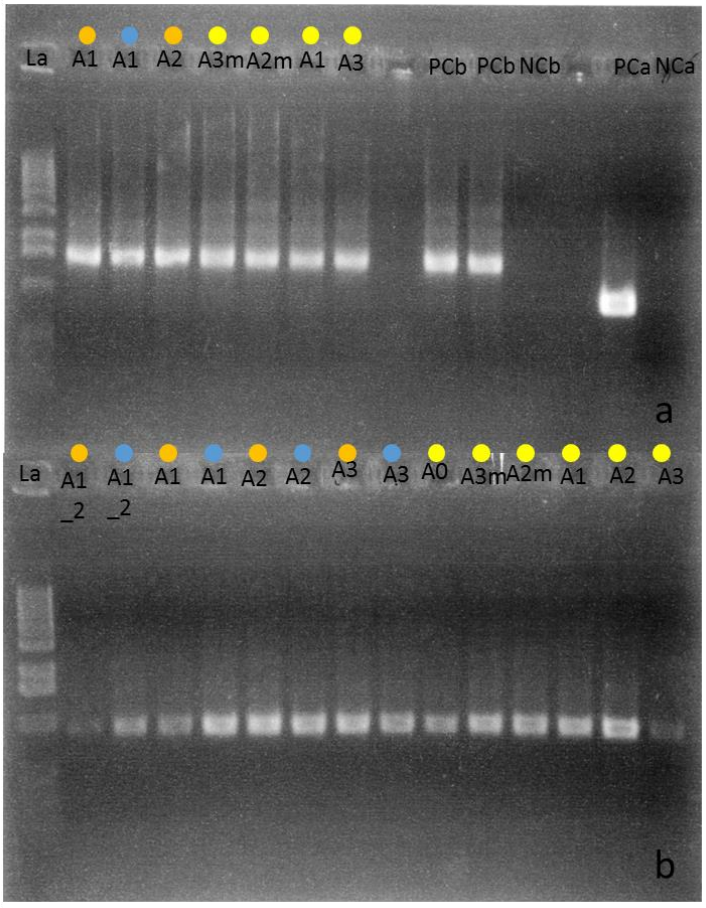

Figure 3.4. Results of PCR for testing the 16S amplification of DNA for sequencing. a) bacterial samples; b) archaeal samples. La, low DNA Mass Ladder; PCb, Positive Bacterial Control; NCb, Negative bacterial Conrol; PCa, Positive Archaeal Control; NCa, Negative archaeal Control. In yellow are the 0-10 cm sediments; in orange the 110 cm sediments; in blue the 410 cm sediments.

Station	Depth bsf cm	DNA Concentration ng/ul	Volume ul	Amount of DNA ng	260/280	260/230
A0	0-5	19.2	10	192.2	1.91	0.03
A1	0-5	21.0	10	209.9	1.85	0.04
A2	0-5	21.8	10	217.6	1.94	0.04
A2m	0-5	17.2	10	171.7	2,00	0.03
A3	0-5	8.0	13	103.9	2.49	0.01
A3m	0-5	13.2	10	132.0	1.9	0.02
A1	110	16.2	10	162.2	1.49	1,00
A2	110	17.6	10	176.1	1.62	0.67
A3	110	18.5	10	185.5	1.62	1.37
A1	410	17.8	10	178.8	1.58	0.5
A2	410	17.0	10	169.9	1.53	0.61
A3	410	18.3	10	183.3	1.61	0.7

Table 3.3. Table that reports DNA concentrations, volume, amount and 260/280 and 260/230 ratios of DNA samples that were shipped for the amplification.

3.4 DNA Sequencing

The extracted DNA was shipped to CeBiTec laboratory (Centrum für Biotechnologie, Universität Bielefeld) and was sequenced with the Illumina MiSeq platform. For 16S amplicon library preparation we used bacterial primers 341F (5´-CCTACGGGNGGCWGCAG-3´) and 785R (5´-GACTACHVGGGTATC TAATCC-3´) and archaeal primers Arch349F (5´-GYGCASCAGKCGMGAAW-3´) and Arch915R (5´-GTGCTCCCCCGCCAATTCCT-3´), which amplified 16S region V3-V4 for Bacteria (length fragment 420 bp) and V4-V6 for Archaea (length fragment 510 bp).

The amplicon library was sequenced with the MiSeq v3 chemistry, in a 2x300 bases paired device. The Illumina sequencing mechanism is, briefly: i) short DNA sequences (adaptors) are attached to the DNA fragments; ii) DNA segments are denatured with sodium hydroxide, and made single stranded; iii) once prepared, the DNA fragments are washed across the flowcell and the complementary DNA binds to primers on the surface of the flowcell whereas the DNA that doesn't attach is washed away; iv) the DNA attached to the flowcell is replicated to form clusters of DNA with the same sequence; these clusters have to be big enough to emit a strong signal that will be detected by a camera; v) unlabelled nucleotide bases and DNA polymerase are added to extend and join the strands of DNA attached to the flowcell. This creates 'bridges' of double-stranded DNA between the primers on the flowcell surface; the double-stranded DNA is then denatured into single-stranded DNA using heat, leaving several million dense clusters of identical DNA sequences; vi) primers and fluorescent labelled terminators, nucleotide bases that stop DNA synthesis, are added to the flowcell; vii) the primer attaches to the DNA being sequenced, vii) the DNA polymerase then binds

to the primer and adds the first fluorescently-labelled terminator to the new DNA strand. Once a base has been added no more bases can be added to the strand of DNA until the terminator base is cut from the DNA; ix) lasers are passed over the flowcell to activate the fluorescent label on the nucleotide base; the fluorescence is detected by a camera and recorded on a computer; each of the terminator (different bases) emits in a different colour; x) the fluorescently-labelled terminator group is then removed from the first base and the next fluorescently-labelled terminator base can bind the DNA stand; this process continues until millions of clusters have been sequenced.

The output of the this sequencing are millions of reverse and forward reads that overlap for a variable number of base pairs, depending on the used primer; in our samples the overlap is about 40-80% for bacteria and about 30% for archaea. Thus the reverse and forward reads had to be merged before to analyze the sequencing date, as well as cleaning and quality control was carried out. The Table 3.4 reports the number of sequences before and after cleaning and merging. First, I removed the primers from the reads with the command-line tool cutadapt (Martin, 2011). Then I used the software TRIMMOMATIC (Bolger et al., 2015) in order to remove the sequences that did not have a good quality; this step has been performed before the reads merging for bacteria and after merging for archaea. The difference in the procedure is due to the different length of the segments (and consequently, the overlapped region between reverse and forward reads). The quality of the sequencing is usually lower at 3'-region of the reads (Bartram et al., 2011), so if there are long fragments, as I have for archaea, it is better performed the trimmomatic step after the merging because these could enhance the number of the holding reads. The merging step was performed with

the PEAR software (Zang et al. 2013). The operational taxonomic unit (OTU) clustering has been made with SWARM (Mahè et al. 2014). OTUs were built with a similarity threshold of 97%. I used this method because the clustering is low influenced by clustering parameters and products robust OTUs. The taxonomic classification is based on SILVA database (Quast et al., 2013). During this step, sequences with less than 90% of similarity with SILVA sequences have been removed; this removal was done in order to remove the presence of amplification and sequencing artifacts, as chimera; the weakness of this approach is the high probability to exclude unknown organisms.

a

	0-5						110			410		
	A0	A1	A2	A2m	A3	A3m	A1	A2	A3	A1	A2	A3
Reads*	87522	123394	59037	55752	39162	54320	169752	159425	92251	48417	115178	146723
Clipped reads*	83590	118163	56328	53224	37440	51852	162567	152438	88613	46317	110355	140707
Trimmed reads*	83558	118126	56312	53195	37431	51833	162498	152383	88574	46295	110324	140663
Assembled reads	82921	117610	56083	52985	37130	51583	161040	151510	88019	45941	109743	139931

b

	0-5						110			410		
	A0	A1	A2	A2m	A3	A3m	A1	A2	A3	A1	A2	A3
Reads*	51982	57240	52121	59126	52415	96761	58347	63821	52467	59727	52298	50405
Clipped reads*	32171	39895	33848	38961	40481	71740	46766	44516	41141	49139	37144	38872
Assembled reads	27023	33308	28817	33633	30577	58977	27556	31290	30787	32840	28368	30339
Trimmed reads	3666	3464	3657	6502	10456	11691	2466	5104	3711	4833	2528	4901

Table 3.4. Table with number of reads after every steps of the quality cleaning. *these numbers represent only the reverse or forward reads, as these steps were performed before the reads merging.

3.5 Statistical analysis

All analyses were carried out in the R statistical environment (R Development Core Team, 2009) with the packages vegan (Oksanen et al., 2010) and ggplot2 (Wickham, 2009), as well as with custom R scripts.

The bacterial and archaeal communities of surface and subsurface sediments were analyzed separately. The number of singletons, doubletons and unique OTUs was calculated separately for surface and subsurface. Singletons (SSO)

are defined as the OTUs that are represented with one sequence in the entire dataset; doubletons (DSO) are the OTUs that are presents with two sequences in only one sample; and unique OTU (OTU_{unique}) are OTUs that are present only in one samples but with more than 2 sequences. With absolute percentage (SSO_{abs}, DSO_{abs} and $OTU_{unique\ abs}$) I refer to number of singletons, doubletons and unique OTUs present in a sample relative to total number of OTUs of the surface or subsurface dataset, whereas with relative percentage (SSO_{rel}) I refer to the contribution of singletons present in a certain sample to total number of OTUs for that sample.

Inverse Simpson (InvS), Exponential Shannon (ExpS), and Chao1 were calculated on a subsampled community to minimize the influence of errors due to the DNA amplification and sequencing. Subsampling was performed randomly taking in consideration the minor number of sequences (30826 for Bacteria and 2073 for Archaea). In order to assess if the subsampling invalidated Chao1, ExpS, InvS indexes and the nOTU, Mantel tests were performed on Eucliden matrixes calculated on those indexes values (calculated with and without subsampling). Furthermore, to calculate if the community structure (CS) between subsampled and not sampled dataset changed, Mantel test was performed on a Bray-Curtis dissimilarity matrix.

To study the diversity between different samples, beta diversity was calculated applying Jaccard index on OTUs presence/absence matrix. Thus the beta-diversity is here a OTUs turnover, showing the number of OTUs shared amongst samples.

The other analyses where performed on the dominant community, here defined as the community without the presence of singletons. Non-metric

multidimensional scaling (nMDS) scatterplots have been performed with average method at OTUs and every taxa levels in order to visualize the main clusters and patterns of the dataset.

Similarity Percentages (SIMPER) analysis was performed on OTU dataset to identify the main OTUs responsible of differences observed in nMDS plot.

As the SIMPER analysis tends to underlines the most abundant objects that are responsible for the observed dissimilarity, an in-depth analysis of the dataset was performed in order to detect all the interesting taxa. Particular importance was given to those taxa that were exclusively, or mainly present in A3 or that showed a decrease abundance from A3 to A0. In addition, in order to have results less biased as possible, I inspected taxa that showed highest relative abundances in A0.

Taxa analyses were carried out with BLAST software (Camacho et al., 2009) and the construction of phylogenetic trees.

3.6 Phylogenetic Tree's Construction

The phylogenetic trees were constructed with Arb software (Ludwig et al., 2004) for those taxa that were highlighted by SIMPER or that showed important changes in relative abundance between areas. The aim of my phylogenetic trees was to see where the prokaryotes more phylogenetically related to my sequences where isolated and if metabolic information were available. The latter is a critical issue, since microbial community of deep sea ecosystems are barely studied and really few organisms have already been cultured (Sogin et al., 2006) so metabolic information were not present for the majority of taxa present in my dataset.

First, the sequences of the studied taxon were aligned with SINA aligner (Pruesse et al., 2012); then they were added to the Silva tree with Parsimony method.

Closest reference sequences were selected and used to build a new tree with Maximum Likelihood method with bootstrap statistical analysis (500 repetitions); the used software was RAxML 8 (Stamatakis, 2014).

Once, constructed the tree backbone with the referenced sequences, my sequences were added with Parsimony method, without any change in the tree topology.

I applied this procedure because the Illumina 16S tag sequencing produces sequences too short (<550 bp) to allow the construction of a solid backbone tree, which, for this reason, was built using only 16S segments longer than 900 bp.

Furthermore, because the taxonomy of the family DHVEG-6 changed recently (Eme and Doolittle, 2015), for this archaeal family I choose to build a second phylogenetic tree. The procedure for the construction of this tree has been the same but, as reference sequences, I selected only organisms previously cultured (Castelle et al., 2005). This approach allowed to better inferring about potential metabolism of OTUs belonging this taxon.

The phylogenetic trees were ultimate in the R statistical environment (R Development Core Team, 2009) with the packages phyloseq (McMurdie and Holmes, 2014), ade (Paradis et al., 2004), ggplot2 (Wickham, 2009), stringi (Gagolewski and Tartanus, 2015) and plyr (Hadley, 2011).

4. Results

Since the rare biosphere (i.e. singletons) represented the large fraction of total OTUs and the number of sequences recovered showed an high variability between samples (Table 4.1; Table 4.2), thus subsampling of Illumina sequences was performed in order to normalize the dataset and therefore to have a better comparison of alpha-diversity between samples.

Mantel test, showing a high correlation between alpha-diversity indexes and community composition calculated on the whole dataset and the subsampling dataset (Table 4.3), highlighted that the bacterial and archaeal diversity and community structure in the subsampling dataset reflected the patterns observed for whole dataset. For this reason, differences in bacterial and archaeal community composition were analysed on whole dataset. Furthermore the rare biosphere (i.e. the singleton component) was not taken into account for analysis of differences in community composition. Conversely, to be conservative, in the following section I described the OTU richness (number of OUTs) for whole dataset and diversity indices (i.e. Chao1, Exponential-Shannon and Inverse-Simpson) for subsampled dataset. Instead sequence number (nSeq), single-sequence OTU or singleton (SSO), double-sequence OUT or doubleton (DSO) and unique OTU (OTU_{unique}) were referred to whole dataset.

4.1 Bacterial Diversity

4.1.1 Comparison between surface and subsurface

The sequencing dataset showed a variable number of sequences amongst different samples (Table 4.1). In general, the sequence number was higher in subsurface samples than in surface samples.

a

	0-5 cm						Tot
	A0	A1	A2	A2m	A3	A3m	
nSEQ	80637	112328	53776	50510	30826	45910	373987
nOTU	27721	31079	18347	16378	9264	14610	98710
SSO	23146	23070	12324	10971	6047	10191	
SSO_{abs} (%)	23.45	23.37	12.49	11.11	6.13	10.32	
SSO_{rel} (%)	83.50	74.23	67.17	66.99	65.27	69.75	
DSO	376	705	186	206	275	460	
DSO_{abs} (%)	0.38	0.71	0.19	0.21	0.28	0.47	
OTU_{unique}	330	356	74	82	304	517	
$OTU_{unique\ abs}$ (%)	0.33	0.36	0.07	0.08	0.31	0.52	
Subsampling							
nOTU	12100	11343	11872	11120	9264	10715	
Chao1	95973	50049	57113	53657	41439	51152	
InvS	285.43	663.45	888.37	703.37	454.89	586.43	
ExpS	2752.97	3325.77	3915.25	3174.53	2174.39	2880.82	

b

	110 cm			410 cm			Tot
	A1	A2	A3	A1	A2	A3	
nSEQ	145953	141502	78211	41852	104178	126448	638144
nOTU	24732	23900	13264	11710	19929	21861	104839
SSO	21545	19504	10178	9163	16771	18137	
SSO_{abs} (%)	20.55	18.60	9.71	8.74	16.00	17.30	
SSO_{rel} (%)	87.11	81.61	76.73	78.25	84.15	82.97	
DSO	291	410	230	123	202	387	
DSO_{abs} (%)	0.28	0.39	0.22	0.12	0.19	0.37	
OTU_{unique}	971	609	208	98	241	344	
$OTU_{unique\ abs}$ (%)	0.93	0.58	0.20	0.09	0.23	0.33	
Subsampling							
nOTU	6724	6982	6257	9027	7082	6761	
Chao1	42112	34914	34929	74467	50125	41660	
InvS	92.63	64.61	55.25	113.34	38.02	47.26	
ExpS	653.12	610.01	459.22	1058.43	517.80	478.38	

Table 4.1. Description of bacterial number of sequences, richness, alpha-diversity and rare biosphere at each site. a) surface layers; b) subsurface layers. nSEQ, total number of sequences; nOTU, number of OTUs; SSO, number of singletons; SSO_{abs}, percentage of singletons relative to total number of OTUs; SSO_{rel}, percentage of singletons relative to number of OTUs of each sample; DSO, number of doubletons; DSO_{abs}, percentage of doubletons relative the total number of OTUs; OTU_{unique}, number of unique OTU; $OTU_{unique\ abs}$: percentage of unique OTUs relative to total number of OTUs. InvS, Inverse Simpson index; ExpS, exponential Shannon index. Subsampling was performed using the minimum bacterial sequences value (30826).

a

	0-5 cm						
	A0	A1	A2	A2m	A3	A3m	Tot
nSEQ	3433	3239	3442	6348	6936	9036	32434
nOTU	1704	1610	1699	2962	3694	4349	15463
SSO	1629	1502	1598	2859	3352	4044	
SSO_{abs} (%)	10.53	9.71	10.33	18.49	21.68	26.15	
SSO_{rel} (%)	95.60	93.29	94.06	96.52	90.74	92.99	
DSO	4	2	0	1	47	39	
DSO_{abs} (%)	0.03	0.01	0.00	0.01	0.30	0.25	
OTU_{unique}	8	1	1	0	78	26	
$OTU_{unique\ abs}$ (%)	0.05	0.01	0.01	0.00	0.50	0.17	
Subsampling							
nOTU	806	814	811	781	971	844	
Chao1	36049	21475	19506	21941	8827	13316	
InvS	65.38	56.15	45.07	43.63	111.58	32.11	
ExpS	261.60	271.62	248.24	226.02	511.97	243.18	

b

	110 cm			410 cm			
	A1	A2	A3	A1	A2	A3	Tot
nSEQ	1565	3257	2746	3345	2073	4115	17101
nOTU	1058	1716	1646	1802	1133	1715	8724
SSO	986	1617	1556	1677	1053	1608	
SSO_{abs} (%)	11.30	18.54	17.84	19.22	12.07	18.43	
SSO_{rel} (%)	93.19	94.23	94.53	93.06	92.94	93.76	
DSO	4	9	5	14	1	9	
DSO_{abs} (%)	0.05	0.10	0.06	0.16	0.01	0.10	
OTU_{unique}	3	14	5	9	1	8	
$OTU_{unique\ abs}$ (%)	0.03	0.16	0.06	0.10	0.01	0.09	
Subsampling							
nOTU	1058	857	964	885	865	691	
Chao1	30676	20666	27118	20308	32725	14960	
InvS	141.13	54.00	59.03	64.56	43.46	23.53	
ExpS	540.37	282.16	363.67	347.93	270.97	142.59	

Table 4.2. Description of archaeal number of sequences, richness, alpha-diversity and rare biosphere at each site. a) surface layers; b) subsurface layers. nSEQ, total number of sequences; nOTU, number of OTUs; SSO, number of singletons; SSO_{abs}, percentage of singletons relative to total number of OTUs; SSO_{rel}, percentage of singletons relative to number of OTUs of each sample; DSO, number of doubletons; DSO_{abs}, percentage of doubletons relative the total number of OTUs; OTU_{unique}, number of unique OTU; $OTU_{unique\ abs}$: percentage of unique OTUs relative to total number of OTUs. InvS, Inverse Simpson index; ExpS, exponential Shannon index. Subsampling was performed using the minimum bacterial sequences value (2073).

	Bacteria		Archaea	
Test	r	p	r	p
CS	0.96	0.001	0.96	0.001
Chao1	0.96	0.001	0.98	0.001
ExpS	0.82	0.0005	0.95	0.001
InvS	0.86	0.001	0.67	0.014
nOTU	0.99	0.001	1.00	0.001

Table 4.3. Mantel test performed on bacterial and archaea entire datasets and subsampled dataset. Mantel test on CS (Community Structure) has been performed on Euclidean distances matrix calculated on Bray-Curtis dissimilarity matrix; whereas, Mantel tests on Chao1 index, ExpS (Exponential Shannon) index, InvS (InverseSimpson) index and nOTU (number of OTUs) have been performed on Euclidean distance matrixes.

The lowest number of sequences was found in the superficial sample A3 (30826 sequences) and the highest value was shown in the sample A1 (145953 sequences), collected at 410 cm bsf. The number of OTUs was also variable between samples, with maximum value at the surface sample A1 (31079 OTUs) and the minimum value at the surface sample A3 (9264 OTUs). The singleton percentages per sample (SSO_{rel}) were higher in subsurface, ranged between 76% and 87%, than in surface samples, ranged between 65% and 83%. Lowest Chao1 was found at 110 cm in all areas (ranged between 34914 and 42112), and the highest values were described for deeper subsurface layer in A1 (74467); superficial samples ranged between 41439 and 57113. Inverse-Simpson (InvS) and Exponential-Shannon (ExpS) indexes are higher in superficial samples (455-888 and 2174-3915 respectively) than subsurface ones (38-113 and 459-1058).

4.1.2 Comparison between areas: surface

The maximum number of sequences and OTUs was found in A1 (112328 and 31079, respectively), whereas the lower values were observed in A3 (30826 and 9264, respectively). The number and relative abundance of singletons decreased from A0 (23146 and 23%, respectively) to A3 (6047-10191 and 6-10%, respectively). The expected richness (Chao1) was higher in A0 than SWIR areas,

with lower richness in A3. InvS and ExpS indexes showed the lowest value in A0 and A3, and the highest in A2 (Table 4.1a).

4.1.3 Comparison between areas: subsurface

At 110 cm bsf we observed a decrease of the number of sequences and OTUs from area 1 to area 3, whereas an opposite trend was found for samples at 410 cm bsf. The SSO_{abs} was highest at A1 for layer 110 cm (20%) and lowest at A1 for layer 410 cm (8%). Chao1, InvS and ExpS were higher in A1 than A2 and A3, in A1 these indices were higher at 410 cm than at 110 cm (Table 4.1b).

4.2 Bacterial Community Composition

The nMDS, performed on OTUs Bray-Curtis similarity matrix, showed two main clusters composed by surface and subsurface samples (Figure 4.1); samples inside these 2 groups had a dissimilarity values under the threshold of 90%. Considering a threshold of 80%, the two superficial A3 samples established a different cluster from the other surface samples; the same happens for the subsurface samples A1. With a dissimilarity threshold of 50% other clusters are formed: two superficial samples, A1 and control area, clustered separately; subsurface samples of Area 1 clustered separately from each other (Figure S1). nMDS performed at taxonomic levels (phylum, class, order, family and genus) showed similar clusters (data not shown). Analysing beta-diversity along the vertical profiles, the highest shared OTUs was between the two subsurface layers, and the value ranged between 15% and 39%. Values between surface and subsurface layers ranged between 0.4-6.5% (110 cm) and between 1.0-4.5% (410 cm). At A3, the number of shared OTUs along vertical profile was highest (6.5%, 39% and 4-4.5%, Figure 4.2c). Analysing horizontal surface profiles, the lowest beta-diversity value was observed amongst A3 other areas (5-14%).

Instead, in the subsurface layers the shared OTUs were higher between A2 and A3 (20%) than between A2 and A1 (13-18%; figure 4.2a).

4.2.1 Subsurface

The Figure 4.3 and Figure 4.4 show the relative abundance of the 10 most abundant families and classes per samples, respectively, and their patterns in areas investigated. At class level the differences between surface and subsurface community's composition were mainly driven by dominance of Dehalococcoida, Candidate division OP8 and Candidate division JS1 in subsurface samples, whereas Gammaproteobacteria, Deltaproteobacteria, Alphaproteobacteria, Flavobacteria and Acidimicrobia were mostly present in superficial samples.

The Candidate division JS1 increased from A1 to A3 in both layers, conversely Dehalococcoida and Candidate division OP8 did not show any consistent patterns between stations and layers. Interesting 9 OTUs belonging to JS1 and 16 OTUs belonging OP8 explained 25%, 25% and 27% of differences between

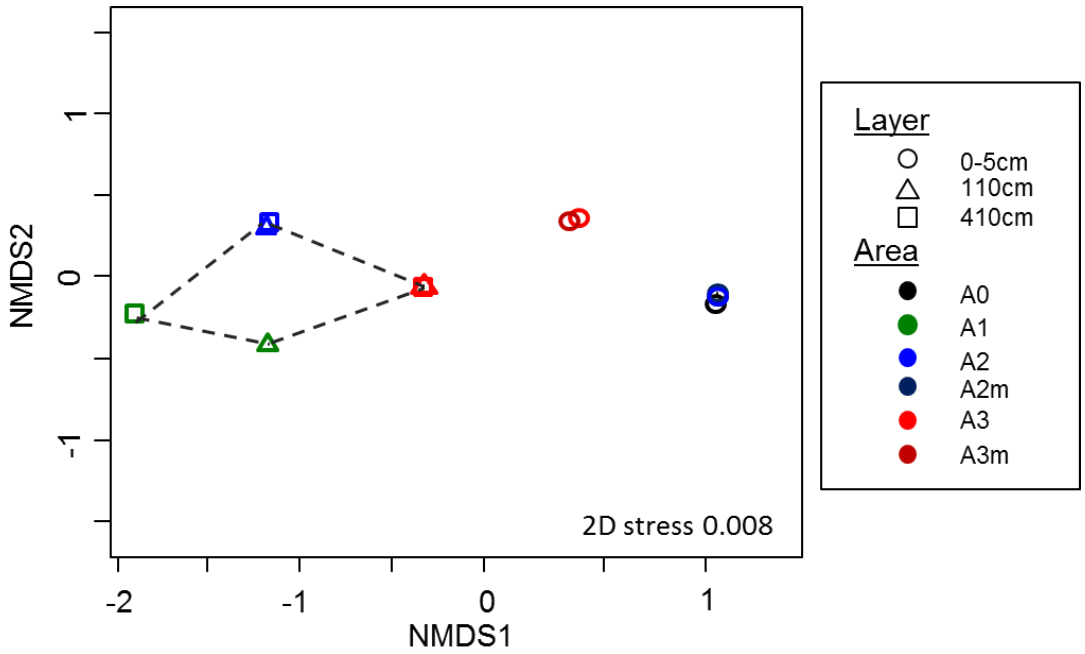

Figure 4.1 Multi-Dimensional Scaling (nMDS) plot performed on bacterial community with average method. The broken line indicates a dissimilarity threshold of 80%.

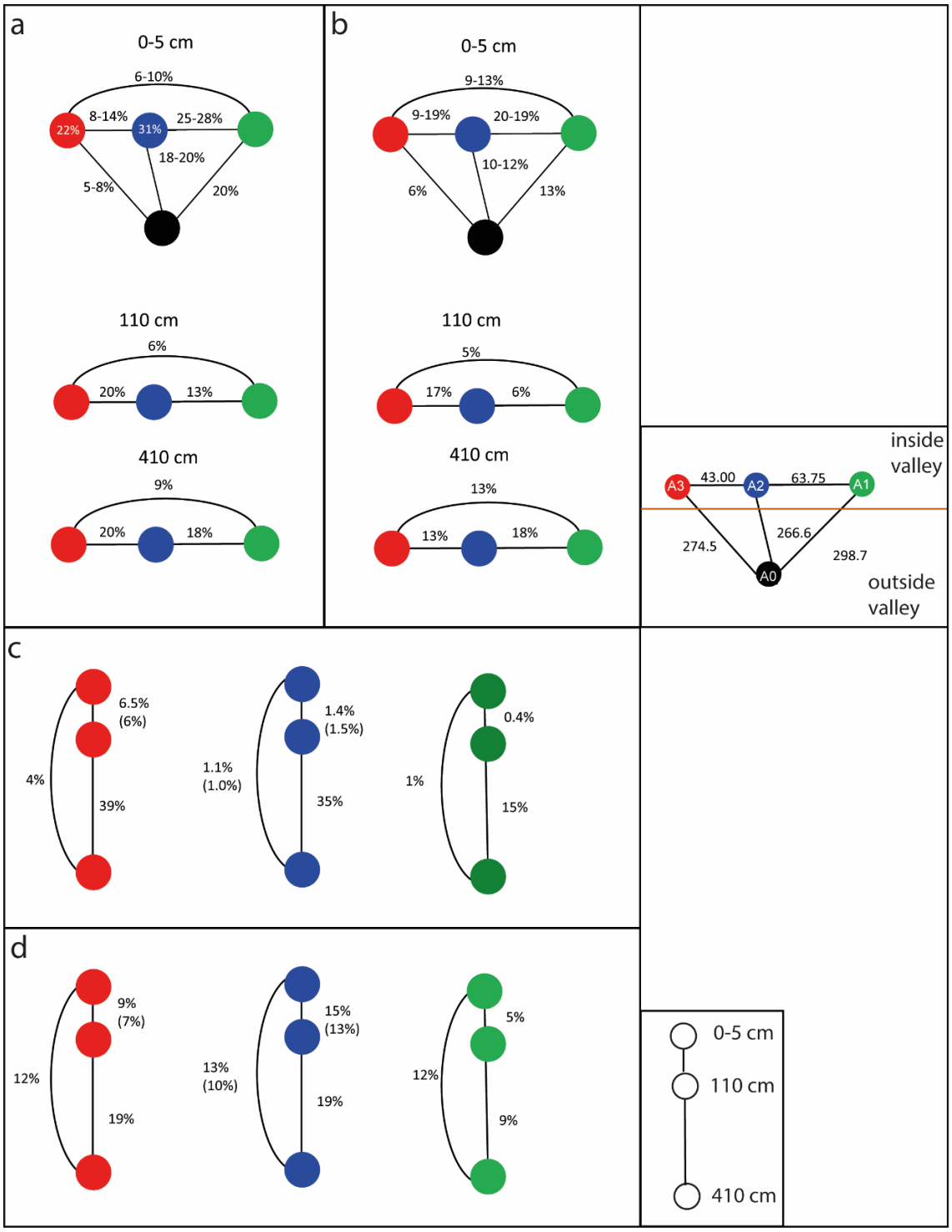

Figure 4.2. Diagram of beta-diversity amongst different stations and layers. Beta-diversity has been calculated applying dissimilarity Jaccard index on OTUs presence/absence matrix. a) bacterial beta-diversity along vertical profiles; b) archaeal beta-diversity along vertical profiles; c) bacterial beta-diversity along horizontal profiles; d) archaeal beta-diversity along horizontal profiles. Values in the brackets refer to A2m and A3m stations.

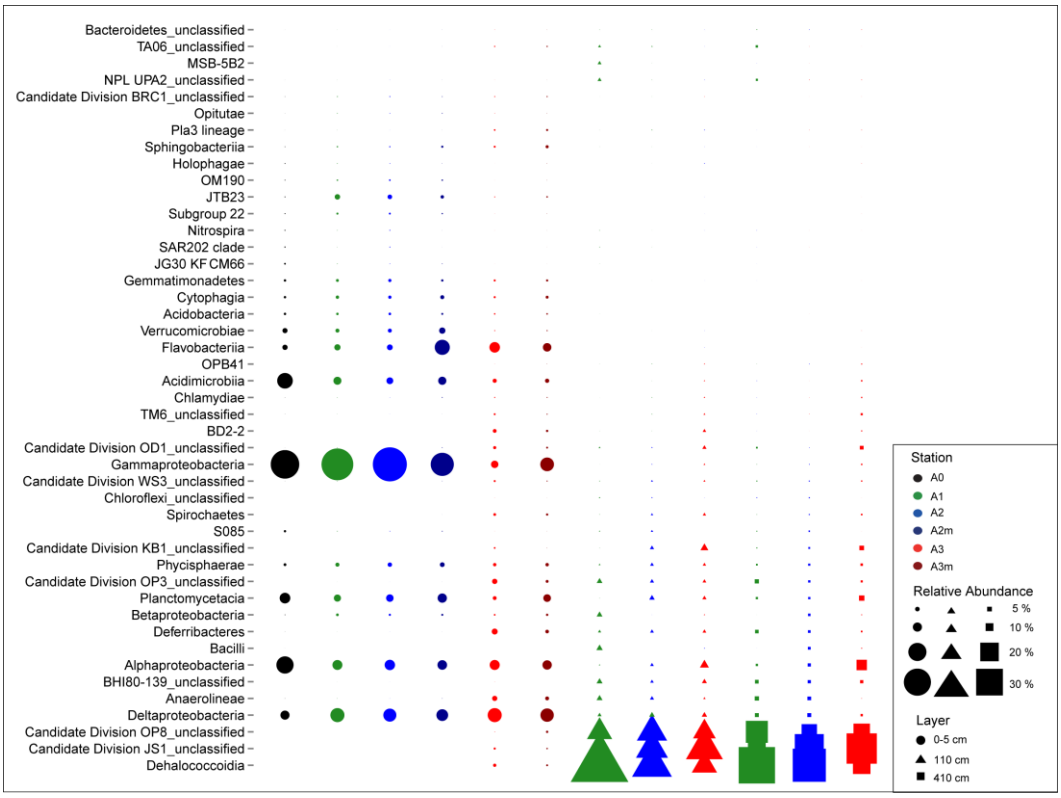

Figure 4.3. Plot representing the 10 most relative abundant bacterial families in each sample.

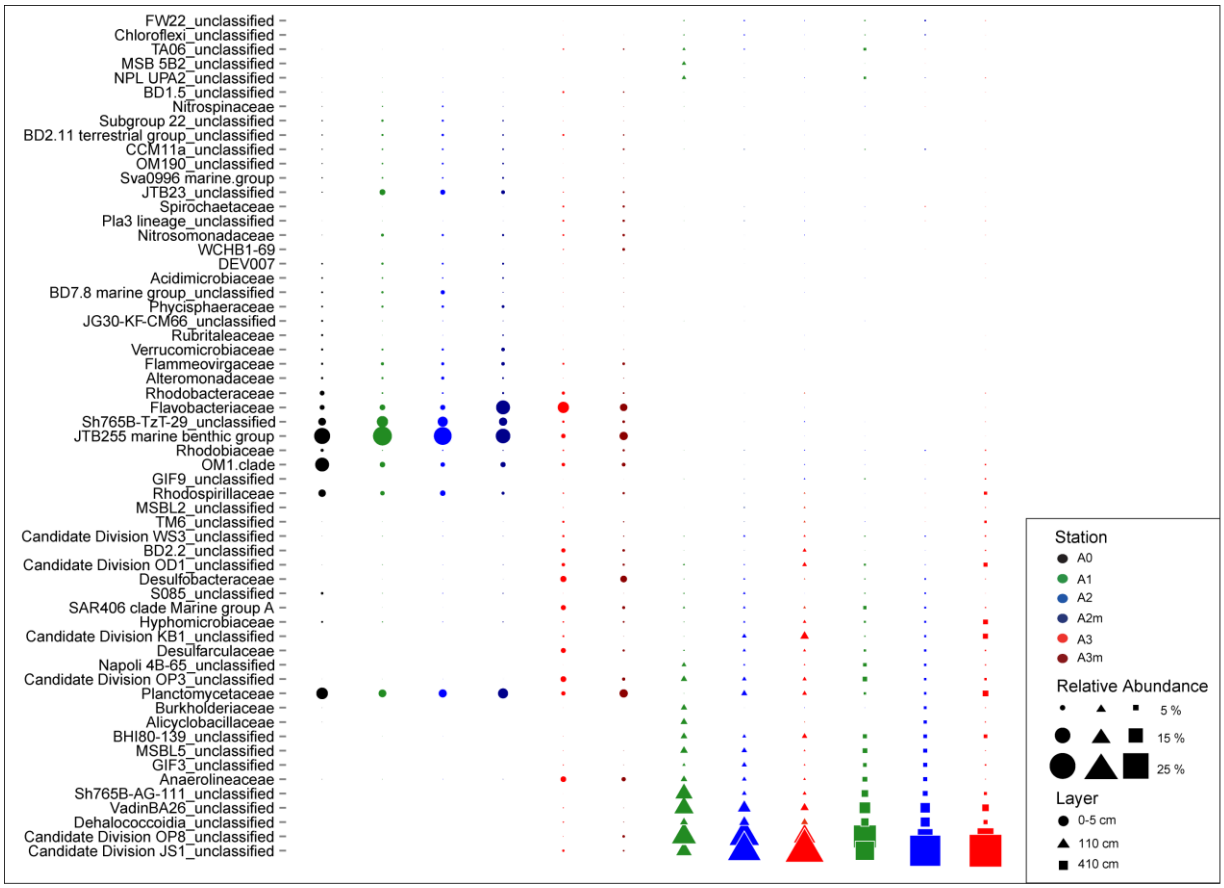

Figure 4.4. Plot representing the 10 most relative abundant bacterial classes in each sample.

A3 and A1, between A2 and A1, and between A3 and A2, respectively (SIMPER; Table S2). Phylogenetic trees of JS1 and OP8 candidate division showed that these OTUs were phylogenetic related to bacterial clones found mainly in seeps, volcanoes and other subsurface ridges (Figure 4.5; Figure 4.6). The OTU55 and OTU105, belonging to the class Dehalococcoidia and explaining 0.8% of the differences between A3 and other areas, showed a higher relative abundance at A3 (2.4% and 1%, respectively) than at A2 and A1 (0.2% and 0.1%, respectively). However the BLAST alignment showed that only OTU105 was close related to Bacteria isolated from chemosynthetic environments (seep and mud volcano).

Four OTUs (OTU77, 17OTU, 40OTU and 146OTU), belonging to Candidate Division KB1, had a relative abundance of 0.6%, 3.3% and 8.5%, respectively in A1, A2 and A3, and in phylogenetic tree they were clustered close to bacteria isolated from methane seeps (Figure 4.7).

4.2.2 Surface

The SIMPER highlighted that 25% of differences between surface community structure at A3 and those at other areas (A0, A1 and A2) were explained by 47 OTUs, 77 OTUs, and 88 OTUs, respectively, belonging to 49 different bacterial taxa (Table S3). Only for those OTUs whose relative abundance was higher at A3 than at A0, A1 and A2 the phylogenetic trees were constructed. The OTUs belonging to SEEP-SRB1 were present only in SWIR areas, and they were close related to bacteria isolated from deep-sea seeps, volcano and ridge habitats (Figure 4.8). In particular the OTU129 had a relative abundance of 0.2% and 1.8% at A3 and A3m, respectively, and explained 0.6-0.7% of differences in nMDS plots between A3 and other areas. The bacterial family JTB255 showed lowest relative abundance in A3 (Figure 4.3), however the relative abundance of

OUT187, belonging to not classified genus of JTB255, was higher at A3 (0.9-1.3%) than at A1 and A2, whereas it was not present A0, and it explained 0.7% of differences in bacterial community structure. The phylogenetic tree clustered this OTU close to bacteria isolated from ridge and hydrothermal systems (data not shown). The OTU224 belonging to bacterial class VC2.1 Bac22 showed a higher relative abundance in A3m (1.1%) than A3 (0.03%) and it was nearly absent in other areas. The phylogenetic tree showed this OTU clustered with an endosymbiont chemolithoautotrophic bacteria (Figure 4.9). The OTU170 and OTU101 belonging to Family SAR406 clade (Marine Group A) were dominant OTUs at A3 (1.6-1.7%, respectively) and explained 1.5-1.7% of differences between bacterial community at A3 and those at A0, A1 and A2. Closer related bacteria were found in marine sulfide deposit and ridge methane seeps (Figure 4.10). Furthermore, the OTU6369 and OTU6594 were found only in A3 surface samples (0.06% and 0.04% in A3 and A3m; respectively), and they were phylogenetically close to chemolithoautotroph bacterial clones. The differences in surficial bacterial community structure were also driven for 0.9-1% by OTU150 and OTU173 (family Anaerolineaceae), whom were present only at A3 (0.4-1%) and related bacteria were found in deep-sea methane and oil rich environments, and ridge fluids (data not shown). The Family Desulfarculaceae was found only in A3, representing 5.3% of bacterial community. In particular the OTU498 and OTU408, contributing to explain 0.3-0.4%, respectively, of SIMPER analysis, were clustered close to bacteria isolated from hydrothermal, mud volcano and oil polluted marine sediments (data not shown). The relative abundance of OTU402 and OTU794, belonging to phylum Candidate Division OP8, was 0.3% and 1.2% at A3 and A3m, respectively, and they were not found in other areas. They

explained 0.3-0.5% of difference in surficial community structure and were clustered close to bacteria isolated from deep-sea sediments and anaerobic methanotrophs isolated from mud-volcano (Figure 4.6). The OUT507, OTU599, OTU698 represented 1.3% of bacterial community at A3m, less than 0.1% in other SWIR areas, and they were not present in reference area. They belonged to family WCHB1-69, and they explained 0.3% of differences between areas. OTU507 and OTU698 clustered close to bacterial clones found in deep sea hydrothermal vent, terrestrial sulphide spring and hypersaline microbial mat. OTU599 clustered close to coral endosymbiont clones (data not shown). The OTUs belonging to subsurface phylum Candidate division JS1 (OTU48, OTU131 and OTU4) were only present in A3, with a relative abundance of 0.9-1.1%, and explained 0.7% of differences between bacterial communities. OTU131 and OTU48 clustered close to mud volcano and anoxic fjord bacterial clones; whereas OTU4 close to subsurface drilling sediment clones (Figure 4.5). Sulfurovum and Sulfurimonas (family Helicobacteraceae) were not selected by SIMPER, however they were exclusively present in A3, with highest relative abundance at A3m (0.9%). These genera include chemolithotrophic bacteria isolated from marine hydrothermal vents and cold seep systems (Figure 4.11).

The genus Spirochaeta showed an abundance of 1.3-1.5% in A3, whereas it is lower in the other areas. The phylogenetic tree showed that the OTUs, here found belonging to this genus, were related to systems of hydrothermal vents and methane seeps (data not shown). The genus Acidiferribacter showed a relative abundance of 0.6% and 0.2% in A3m and A3, respectively, and it was absent in A0; the analysis performed on BLAST platform highlighted its phylogenetic affinity to chemosynthetic organisms.

Furthermore, a crosscheck was carried out on OTUs that were highlighted by the SIMPER and that showed higher relative abundance in A0. The analysed taxa S085, Pseudomonas, Rubritalea, Candidate Division OM1 were found correlated with bacterial clones previously isolated from deep sea sediment.

4.3 Archaeal Diversity

4.3.1 Comparison between surface and subsurface

Superficial samples showed a higher number of sequences than subsurface samples, ranging between 3239-9036 and 1565-4115, respectively (Table 4.2). Number of OTUs showed a similar trend, with 1610-4349 OTUs in surficial samples and 1058-1802 in subsurface samples. The SSO_{rel} was 91-96% and 93-95% for surficial and subsurface samples, respectively. The percentage of OTU_{unique} was lower than 0.2% in all samples. Chao1 ranged between 8827 and 36049 in surface samples, and between 14960 and 32725 subseafloor layers. InvS showed values between 32 and 111 in surface layer and between 23 and 141 in subsurface layers. In surface samples, ExpS had a minimum value of 226 and a maximum value of 512, and it ranged between 143 and 540 in subsurface samples.

4.3.2 Comparison between areas: surface

The highest number of sequences and OTUs was observed in A3 (6936-9036 and 3694-4349, respectively) and in the sample A2m (6348 and 2962, respectively); in the other samples these values were less than 3500 sequences and 1800 OTUs. Highest SSO_{abs} was observed in A3 and A3m (22% and 25%; respectively); in other areas, this value ranged between 10% (A0, A1 and A2) and 18% (A2m). Highest Chao1 value was calculated for A0 (36050), inside the SWIR the estimated richness decreased from A1 to A3 (21475-8827). InvS and

ExpS decreased from A0 to A3m (65.4-32.1 and 162-243, respectively), however highest values were observed for A3 (111.6 and 512, respectively; Table 4.2a).

4.3.3 Comparison between areas: subsurface

In A1 and A3 the number of sequences and OTUs increased from 110 cm to 410 cm bsf, whereas an opposite trend was observed for A2. SSO_{abs} didn't show any pattern between areas and layers; this value ranged between 11% and 19%. Chao1 didn´t show any consistent trend between areas and layers. InvS and ExpS were higher at A1 than at A2 and A3, and they decreased from 110 cm to 410 cm (bsf) in all areas (Table 4.2b).

4.4 Archaeal Community Composition

The NMDS plot showed that the A0 clustered separately from SWIR areas with a dissimilarity value of 70% (Figure 4.12). Considering a dissimilarity threshold of 60%, the superficial sample A3 clustered apart from the other samples. Whereas with the 40% of dissimilarity, four other clusters formed: A2 subsurface layers and A1 110 cm layer; A1 410 cm layer; both A3 subsurface layers and A3m surficial layer; A1 and A2 surficial layers (Figure S2).

Beta-diversity along vertical profile of A1 and A3, the surficial layer shared a major number of OUTs with deeper layer (410 cm) than with 110 cm. In A2 the number of OUTs shared between surficial layer and subseafloor layers decreased with sediment depth. In A2 and A3 the shared OTUs between subsurface layers were higher than those shared between surface layer and subsurface layers.

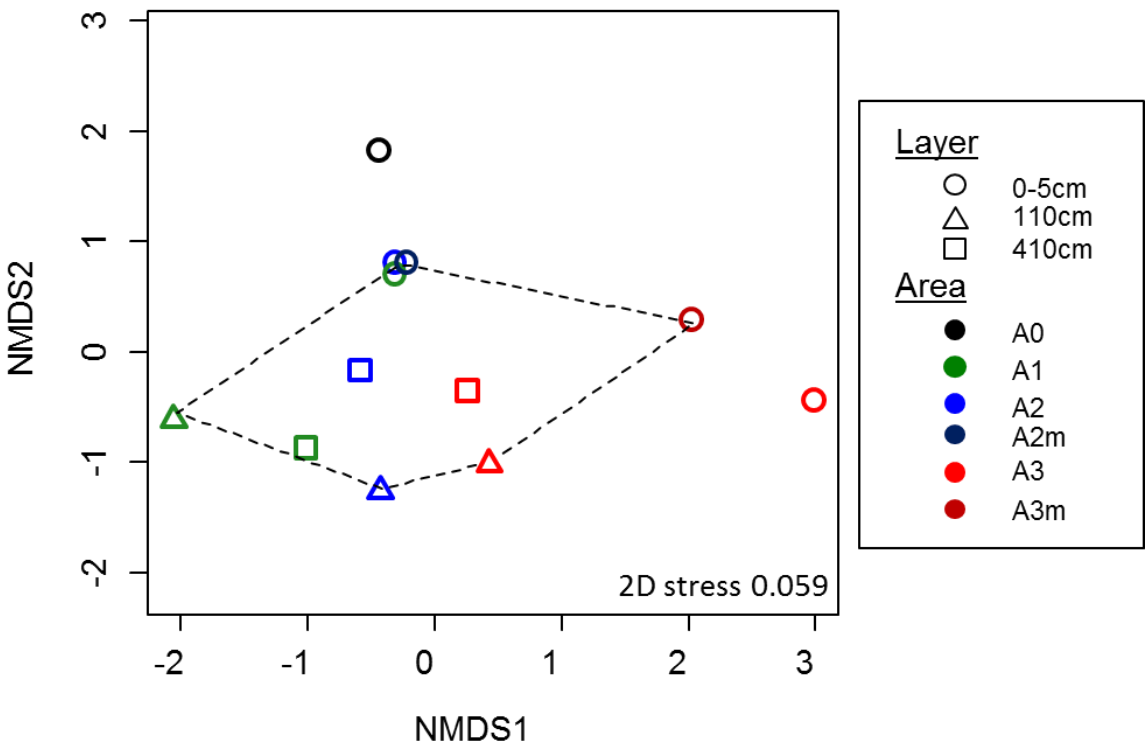

Figure 4.12. Multi-Dimensional Scaling (nMDS) plot performed on archaeal community with average method. The broken line indicates a dissimilarity threshold of 70%.

Conversely, in A1 the shared OTUs between subsurface layers were lower than those shared by surface and 410 cm layers (Figure 4.2d).

The analysis of surficial beta-diversity showed the same pattern observed for bacterial beta-diversity. I observed a lower number of shared OTUs between A2 and A3 than between A2 and A1, and a higher number of shared OTUs between A1 and A0 than between A1 and A3, with lowest OTUs shared between A3 and A0. In the 110 cm layer the beta-diversity decreased with distance between areas, conversely in 410 cm layer the number of shared OTUs between A2 and A3 was higher than between A2 and A1 (Figure 4.2b).

4.4.1 Surface and subsurface

At A0, the archaeal community was dominated by unclassified archaea belonging to Marine Group I and by Candidatus Nitrosopumilus (Figure 4.13). The latter dominated also in surficial and subsurface samples at SWIR areas, with exception for superficial station A3, where the dominant archaeal family was

Deep Sea Hydrothermal Vent Gp 6 (DHVEG-6; 53%). In subsurface layers other two important taxa were Marine Benthic Group D and Deep Sea Hydrothermal Vent Gp 1 (MBGD and DHVEG-1) and Group C3. The highest relative abundance of MBGD and DHVEG-1 was found in A1 (21% in the 110 cm layer and 16% in 410 cm layer); it was about 7% in A2 and 5% in A3. The relative abundance of C3 showed higher values in the deepest layer, here the value ranged between 9% and 12% in contrast with the 110 cm layer where the values ranged between 5% and 8%. Interesting phylogenetic tree showed that the majority of OTUs, belonging to DHVEG-6, clustered close to archaea isolated from hydrothermal and seep environments (Figure 4.14). Likewise, OTUs belonging to MBGD and DHVEG-1 were related to archaea identified in chemosynthetic environments (data not shown). The family Diapherotrites was found exclusively in surficial sediments of A3, and in particular the OTU47, representing 2.7% of archaeal community in the superficial sample of A3, was close to hydrothermal archaea in phylogenetic tree (data not shown). Five OTUs belonging to Marine Hydrothermal Vent Group (MHVG) were also found only at A3 (1.2%) and they were related to archaea described for chemosynthetic and methanogenic environments.

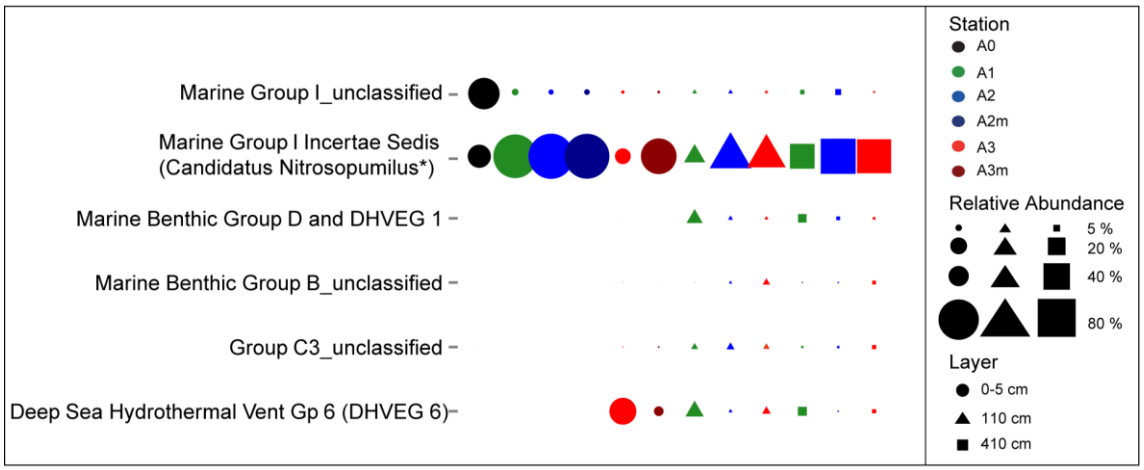

Figure 4.13. Plot representing the most abundant archaeal families in the dataset. *genus level

The phylogenetic tree of Marine Group I showed lack of differential OTUs clustering amongst investigated areas, with related archaea isolated both from deep-sea and hydrothermal systems (data not shown). Furthermore, I analysed OTUs belonging to the genus Candidatus Nitrosopumilus on the BLAST platform and, of particular concern is the OTU1 that was dominant at A3 (with a relative abundance of 27% in A3m), showed a decreasing trend from A2 to A0 (2%) and resulted phylogenetically close to methane-seep archaeal clones.

Figure 4.5. Phylogenetic tree of the phylum Candidate Division JS1. The tree backbone was constructed, including only the reference sequences, with Maximum Likelihood Method and 500 bootstraps were performed; then SWIR JS1 sequences were added with Parsimony Method. SWIR JS1 sequences are bolded. Red writings indicate highlighted OTUs by the SIMPER. (next page)

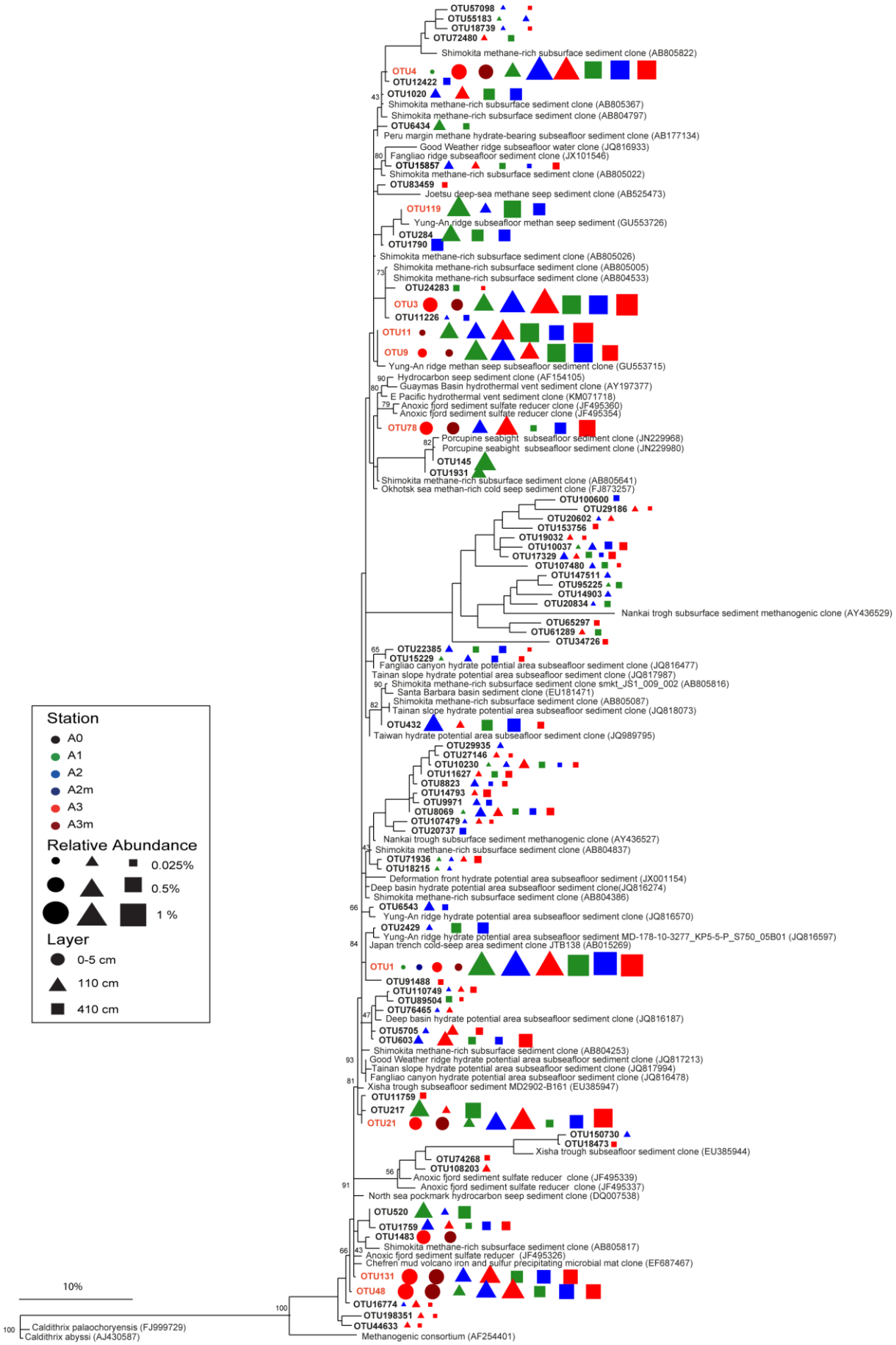
Station
A0
A1
A2
A2m
A3
A3m
Relative Abundance
0.025%
0.5%
1 %
Layer
0-5 cm
110 cm
410 cm
10%
OTU57098
OTU55183
OTU18739
OTU72480
Shimokita methane-rich subsurface sediment clone (AB805822)
OTU4
OTU12422
OTU1020
Shimokita methane-rich subsurface sediment clone (AB805367)
Shimokita methane-rich subsurface sediment clone (AB804797)
OTU6434
Peru margin methane hydrate-bearing subseafloor sediment clone (AB177134)
Good Weather ridge subseafloor water clone (JQ816933)
Fangliao ridge subseafloor sediment clone (JX101546)
OTU15857
Shimokita methane-rich subsurface sediment clone (AB805022)
OTU83459
Joetsu deep-sea methane seep sediment clone (AB525473)
OTU119
Yung-An ridge subseafloor methan seep sediment (GU553726)
OTU284
OTU1790
Shimokita methane-rich subsurface sediment clone (AB805026)
Shimokita methane-rich subsurface sediment clone (AB805005)
Shimokita methane-rich subsurface sediment clone (AB804533)
OTU24283
OTU3
OTU11226
OTU11
OTU9
Yung-An ridge methan seep subseafloor sediment clone (GU553715)
Hydrocarbon seep sediment clone (AF154105)
Guaymas Basin hydrothermal vent sediment clone (AY197377)
E Pacific hydrothermal vent sediment clone (KM071718)
Anoxic fjord sediment sulfate reducer clone (JF495360)
Anoxic fjord sediment sulfate reducer clone (JF495354)
OTU78
Porcupine seabight subseafloor sediment clone (JN229968)
Porcupine seabight subseafloor sediment clone (JN229980)
OTU145
OTU1931
Shimokita methane-rich subsurface sediment clone (AB805641)
Okhotsk sea methan-rich cold seep sediment clone (FJ873257)
OTU100600
OTU29186
OTU20602
OTU153756
OTU19032
OTU10037
OTU17329
OTU107480
OTU147511
OTU95225
OTU14903
OTU20834
Nankai trogh subsurface sediment methanogenic clone (AY436529)
OTU65297
OTU61289
OTU34726
OTU22385
OTU15229
Fangliao canyon hydrate potential area subseafloor sediment clone (JQ816477)
Tainan slope hydrate potential area subseafloor sediment clone (JQ817987)
Shimokita methane-rich subsurface sediment clone smkt_JS1_009_002 (AB805816)
Santa Barbara basin sediment clone (EU181471)
Shimokita methane-rich subsurface sediment clone (AB805087)
Tainan slope hydrate potential area subseafloor sediment clone (JQ818073)
OTU432
Taiwan hydrate potential area subseafloor sediment clone (JQ989795)
OTU29935
OTU27146
OTU10230
OTU11627
OTU8823
OTU14793
OTU9971
OTU8069
OTU107479
OTU20737
Nankai trough subsurface sediment methanogenic clone (AY436527)
Shimokita methane-rich subsurface sediment clone (AB804837)
OTU71936
OTU18215
Deformation front hydrate potential area subseafloor sediment (JX001154)
Deep basin hydrate potential area subseafloor sediment clone(JQ816274)
Shimokita methane-rich subsurface sediment clone (AB804386)
OTU6543
Yung-An ridge hydrate potential area subseafloor sediment clone (JQ816570)
OTU2429
Yung-An ridge hydrate potential area subseafloor sediment MD-178-10-3277_KP5-5-P_S750_05B01 (JQ816597)
Japan trench cold-seep area sediment clone JTB138 (AB015269)
OTU1
OTU91488
OTU110749
OTU89504
OTU76465
Deep basin hydrate potential area subseafloor sediment clone (JQ816187)
OTU5705
OTU603
Shimokita methane-rich subsurface sediment clone (AB804253)
Good Weather ridge hydrate potential area subseafloor sediment clone (JQ817213)
Tainan slope hydrate potential area subseafloor sediment clone (JQ817994)
Fangliao canyon hydrate potential area subseafloor sediment clone (JQ816478)
Xisha trough subseafloor sediment MD2902-B161 (EU385947)
OTU11759
OTU217
OTU21
OTU150730
OTU18473
Xisha trough subseafloor sediment clone (EU385944)
OTU74268
OTU108203
Anoxic fjord sediment sulfate reducer clone (JF495339)
Anoxic fjord sediment sulfate reducer clone (JF495337)
North sea pockmark hydrocarbon seep sediment clone (DQ007538)
OTU520
OTU1759
OTU1483
Shimokita methane-rich subsurface sediment clone (AB805817)
Anoxic fjord sediment sulfate reducer (JF495326)
Chefren mud volcano iron and sulfur precipitating microbial mat clone (EF687467)
OTU131
OTU48
OTU16774
OTU198351
OTU44633
Methanogenic consortium (AF254401)
Caldithrix palaochoryensis (FJ999729)
Caldithrix abyssi (AJ430587)

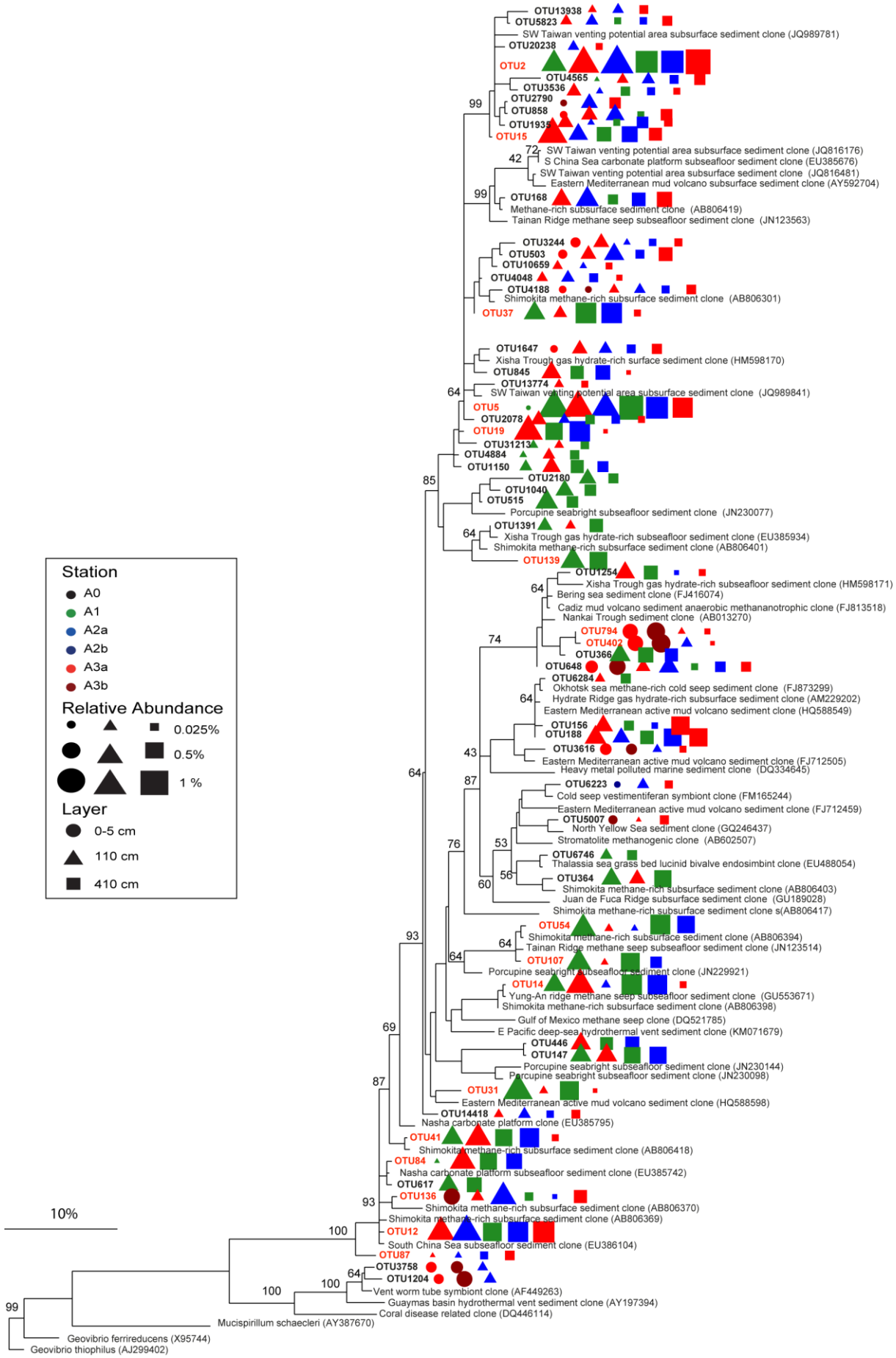
Station
A0
A1
A2a
A2b
A3a
A3b
Relative Abundance
0.025%
0.5%
1 %
Layer
0-5 cm
110 cm
410 cm
10%
OTU13938
OTU5823
SW Taiwan venting potential area subsurface sediment clone (JQ989781)
OTU20238
OTU2
OTU4565
OTU3536
OTU2790
OTU858
OTU1935
OTU15
SW Taiwan venting potential area subsurface sediment clone (JQ816176)
S China Sea carbonate platform subseafloor sediment clone (EU385676)
SW Taiwan venting potential area subsurface sediment clone (JQ816481)
Eastern Mediterranean mud volcano subsurface sediment clone (AY592704)
OTU168
Methane-rich subsurface sediment clone (AB806419)
Tainan Ridge methane seep subseafloor sediment clone (JN123563)
OTU3244
OTU503
OTU10659
OTU4048
OTU4188
Shimokita methane-rich subsurface sediment clone (AB806301)
OTU37
OTU1647
Xisha Trough gas hydrate-rich surface sediment clone (HM598170)
OTU845
OTU13774
SW Taiwan venting potential area subsurface sediment clone (JQ989841)
OTU5
OTU2078
OTU19
OTU31213
OTU4884
OTU1150
OTU2180
OTU1040
OTU515
Porcupine seabright subseafloor sediment clone (JN230077)
OTU1391
Xisha Trough gas hydrate-rich subseafloor sediment clone (EU385934)
Shimokita methane-rich subsurface sediment clone (AB806401)
OTU139
OTU1254
Xisha Trough gas hydrate-rich subseafloor sediment clone (HM598171)
Bering sea sediment clone (FJ416074)
Cadiz mud volcano sediment anaerobic methananotrophic clone (FJ813518)
Nankai Trough sediment clone (AB013270)
OTU794
OTU402
OTU366
OTU648
OTU6284
Okhotsk sea methane-rich cold seep sediment clone (FJ873299)
Hydrate Ridge gas hydrate-rich subsurface sediment clone (AM229202)
Eastern Mediterranean active mud volcano sediment clone (HQ588549)
OTU156
OTU188
OTU3616
Eastern Mediterranean active mud volcano sediment clone (FJ712505)
Heavy metal polluted marine sediment clone (DQ334645)
OTU6223
Cold seep vestimentiferan symbiont clone (FM165244)
Eastern Mediterranean active mud volcano sediment clone (FJ712459)
OTU5007
North Yellow Sea sediment clone (GQ246437)
Stromatolite methanogenic clone (AB602507)
OTU6746
Thalassia sea grass bed lucinid bivalve endosimbint clone (EU488054)
OTU364
Shimokita methane-rich subsurface sediment clone (AB806403)
Juan de Fuca Ridge subsurface sediment clone (GU189028)
Shimokita methane-rich subsurface sediment clone s(AB806417)
OTU54
Shimokita methane-rich subsurface sediment clone (AB806394)
Tainan Ridge methane seep subseafloor sediment clone (JN123514)
OTU107
Porcupine seabright subseafloor sediment clone (JN229921)
OTU14
Yung-An ridge methane seep subseafloor sediment clone (GU553671)
Shimokita methane-rich subsurface sediment clone (AB806398)
Gulf of Mexico methane seep clone (DQ521785)
E Pacific deep-sea hydrothermal vent sediment clone (KM071679)
OTU446
OTU147
Porcupine seabright subseafloor sediment clone (JN230144)
Porcupine seabright subseafloor sediment clone (JN230098)
OTU31
Eastern Mediterranean active mud volcano sediment clone (HQ588598)
OTU14418
Nasha carbonate platform clone (EU385795)
OTU41
Shimokita methane-rich subsurface sediment clone (AB806418)
OTU84
Nasha carbonate platform subseafloor sediment clone (EU385742)
OTU617
OTU136
Shimokita methane-rich subsurface sediment clone (AB806370)
Shimokita methane-rich subsurface sediment clone (AB806369)
OTU12
South China Sea subseafloor sediment clone (EU386104)
OTU87
OTU3758
OTU1204
Vent worm tube symbiont clone (AF449263)
Guaymas basin hydrothermal vent sediment clone (AY197394)
Coral disease related clone (DQ446114)
Mucispirillum schaecleri (AY387670)
Geovibrio ferrireducens (X95744)
Geovibrio thiophilus (AJ299402)

Figure 4.6. Phylogenetic tree of the phylum Candidate Division OP8. The tree backbone was constructed, including only the reference sequences, with Maximum Likelihood Method and 500 bootstraps were performed; then SWIR OP8 sequences were added with Parsimony Method. SWIR OP8 sequences are bolded. Red writings indicate highlighted OTUs by the SIMPER.

(previous page)

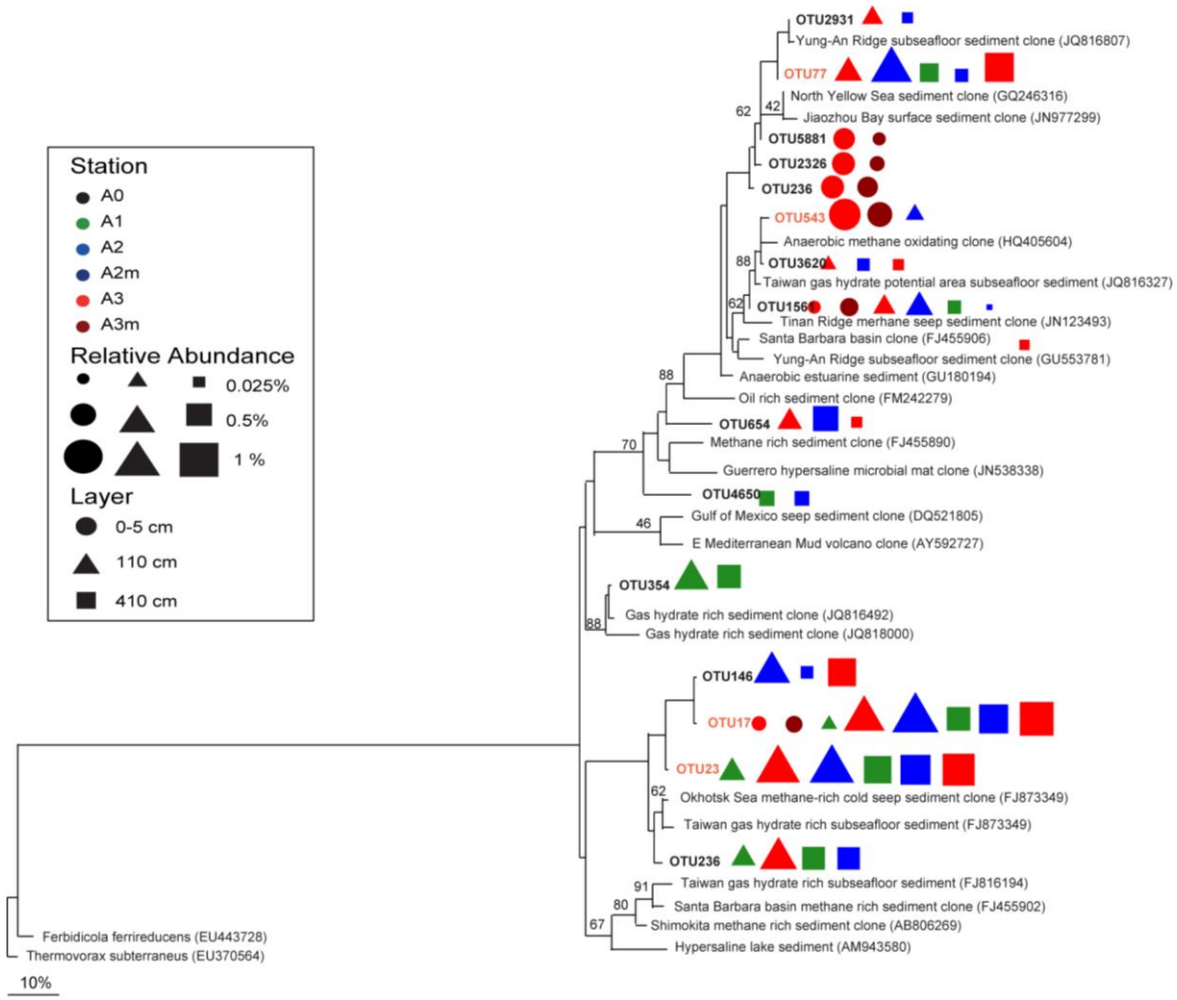

Figure 4.7. Phylogenetic tree of the phylum Candidate Division KB1. The tree backbone was constructed, including only the reference sequences, with Maximum Likelihood Method and 500 bootstraps were performed; then SWIR KB1 sequences were added with Parsimony Method. SWIR KB1 sequences are bolded. Red writings indicate highlighted OTUs by the SIMPER.

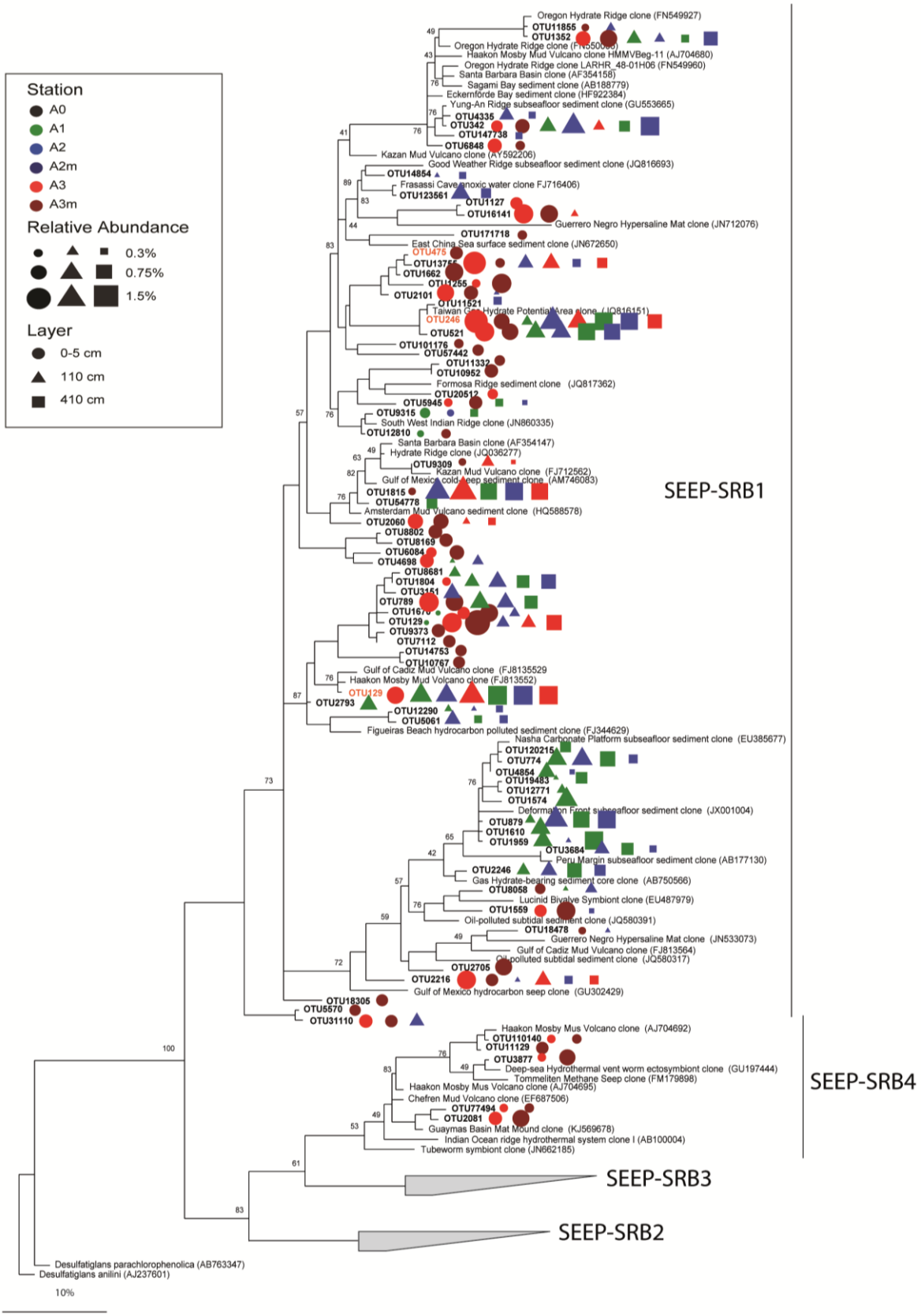

Figure 4.8. Phylogenetic tree of the genus SEEP-srb1. The tree backbone was constructed, including only the reference sequences, with Maximum Likelihood Method and 500 bootstraps were performed; then SWIR SEEP-srb1 sequences were added with Parsimony Method. SWIR SEEP-srb1 sequences are bolded. Red writings indicate highlighted OTUs by the SIMPER.

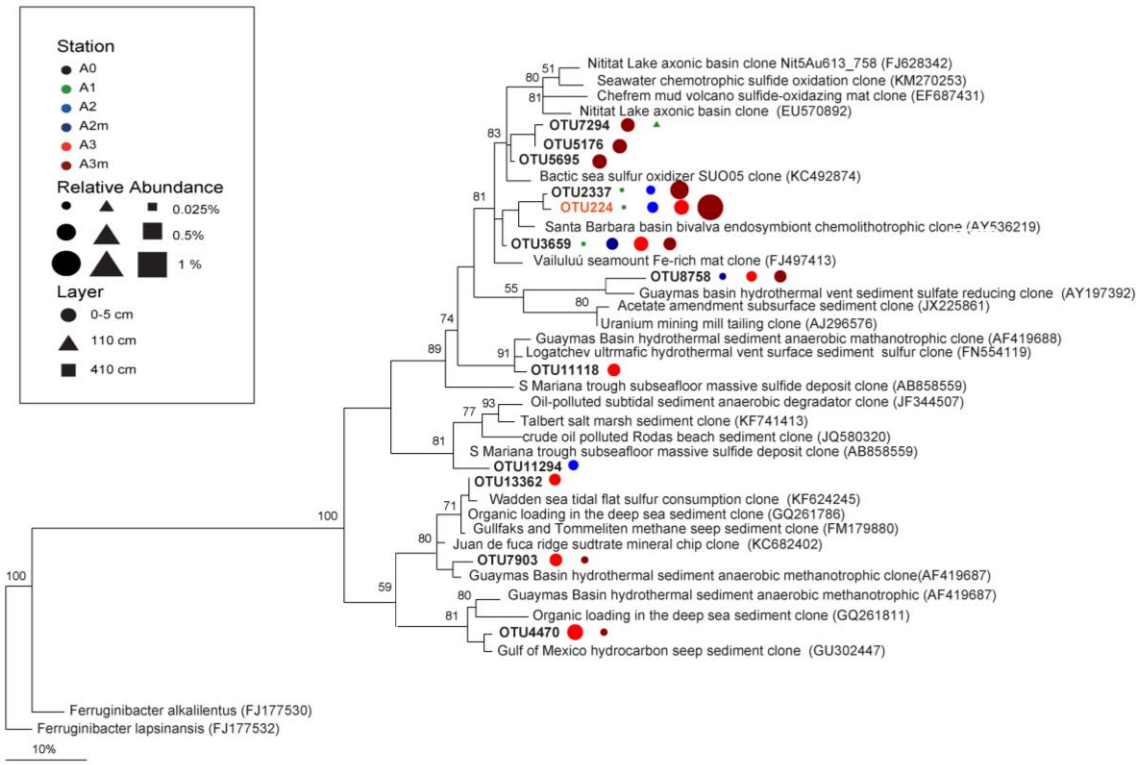

Figure 4.9. Phylogenetic tree of the order VC2.1 Bac22. The tree backbone was constructed, including only the reference sequences, with Maximum Likelihood Method and 500 bootstraps were performed; then SWIR VC2.1 Bac22 sequences were added with Parsimony Method. SWIR VC2.1 Bac22 sequences are bolded. Red writings indicate highlighted OTUs by the SIMPER.

Figure 4.10. Phylogenetic tree of the family Sar406. The tree backbone was constructed, including only the reference sequences, with Maximum Likelihood Method and 500 bootstraps were performed; then SWIR Sar406 sequences were added with Parsimony Method. SWIR Sar406 sequences are bolded. Red writings indicate highlighted OTUs by the SIMPER.

(next page)


Station
A0
A1
A2a
A2b
A3a
A3b
Relative Abundance
0.025%
0.5%
1 %
Layer
0-5 cm
110 cm
410 cm
Marinimicrobia
(SAR406 clade)
LCP-89
PAUC34f
10%
OTU170
OTU8789
OTU732
Southern Mariana Trough sulfide deposit clone(AB858637)
OTU76435
OTU101
OTU252
Yung-An Ridge methane seep clone(GU553712)
OTU6570
OTU15215
OTU108451
OTU98
OTU2952
SW Taiwan gas hydrate potential area clone(JX001082)
OTU1745
Eel River Basin methane seep sediment clone (FJ264664)
Eel River Basin methane seep sediment clone (FJ264782)
OTU8763
Tommeliten methane seep clone (FM179905)
OTU25243
Svalbard arctic fjord sediment clone (CQ259264)
Southern Mariana Trough sulfide deposit clone (AB858515)
Loi'hi Seamount Pisces Peak lavas sediment clone (EU491156)
OTU8581
OTU6590
OTU4063
Manantial del Toro hypersaline groundwater clone (JF747697)
Chefren Mud Vulcano sulfide-oxidizing mat sediment clone (EF687280)
Southern Mariana Trough sulfide deposit clone (AB722155)
OTU2451
OTU707
OTU16758
Lake Kauhako (Hawaii) water clone (AY344400)
Sawmill Sink water column clone (FJ716274)
OTU12433
OTU5204
Northeast Subartic Pacific Ocean sediment clone (HQ672811)
OTU573
OTU3395
OTU3360
OTU20861
OTU405
Arabian Sea water clone (KJ589871)
OTU9457
Northeast Subartic Pacific Ocean water clone (HQ674365)
OTU9107
OTU6885
OTU2072
Formosa Ridge subseafloor sediment clone (JQ817428)
OTU553
OTU88339
SW Taiwan gas hydrate potential area clone (JX001150)
OTU5279
OTU4885
Abyssal subsurface clone (JN676029)
Shimokita offshore drilling core clone (AB806185)
OTU3194
OTU13130
Nansha carbonate platform subsurface sediment clone (EU385761)
Shimokita offshore drilling core clone (AB806183)
Clarion-Clipperton Fracture Zone polymetallic nodule clone(JX227098)
OTU60958
Okinawa Trough sediment clone (KC470910)
Baltic Sea redoxcline clone (KC492866)
Saanich Inlet chemolithoautotroph clone (GQ348467)
Saanich Inlet chemolithoautotroph clone (GQ347640)
OTU6369
OTU6594
OTU171543
OTU5495
OTU76681
Anaerobic Reactor digester bacteria community clone (AF275926)
Shaban Deep brine-seawater interface clone (AJ347758)
OTU908
Abyssal subsurface clone (JN675973)
OTU226
OTU12625
Pacific Ocean Margin methane hydrathe sediment clone (AB177206)
OTU22
OTU11175
OTU912
Clipperton atoll stratified lagoon clone (HQ691901)
OTU9974
Guerrero Negro hypersaline mat clone (JN461109)
Anaerobic sludge digester clone (CR933118)
Anaerobic sludge digester clone (CR933119)
OTU60172
OTU7649
South Pacific Gyre oligotrophic abyssal sediment clone (HQ721395)
OTU10141
South Pacific abissal sediment clone (FJ746114)
OTU16231
Highborne Cay oolitic sand clone (JX504390)
OTU870
OTU2630
OTU565
OTU142
South China Sea subseafloor sediment clone (EU386122)
OTU6281
Anoxic Fjord sediment clone (JF495371)
OTU1779
OTU161689
OTU12277
OTU302
South China Sea sediment clone (EU048684)
OTU13481
OTU3589
OTU898
Bahamas Sawmill Sink water clone (FJ716279)
French Guiana shallow mud clone (KC009954)
High-pressure reactor sulfate-reducing clone (HF922356)
OTU7409
High-pressure reactor sulfate-reducing clone (HF922356)
Sulfate-reducing cave biofilm clone (FJ716412)
OTU441
OTU610
Lucinid bivalve symbiont clone (EU487873)
OTU12966
OTU19136
OTU19076
Anoxic Fjorrd sediment clone (JF495370)
Caldithrix abyssi DSM 13497 (AGCQ01000003)
Caldithrix palaeochoryensis (FJ999729)
Chlamydophila abortus (AB001783)
Chlamydophila psittaci (U68447)
Chlamydophila caviae GPIC (AE015925)
Chlamydophila felis (DB5701)

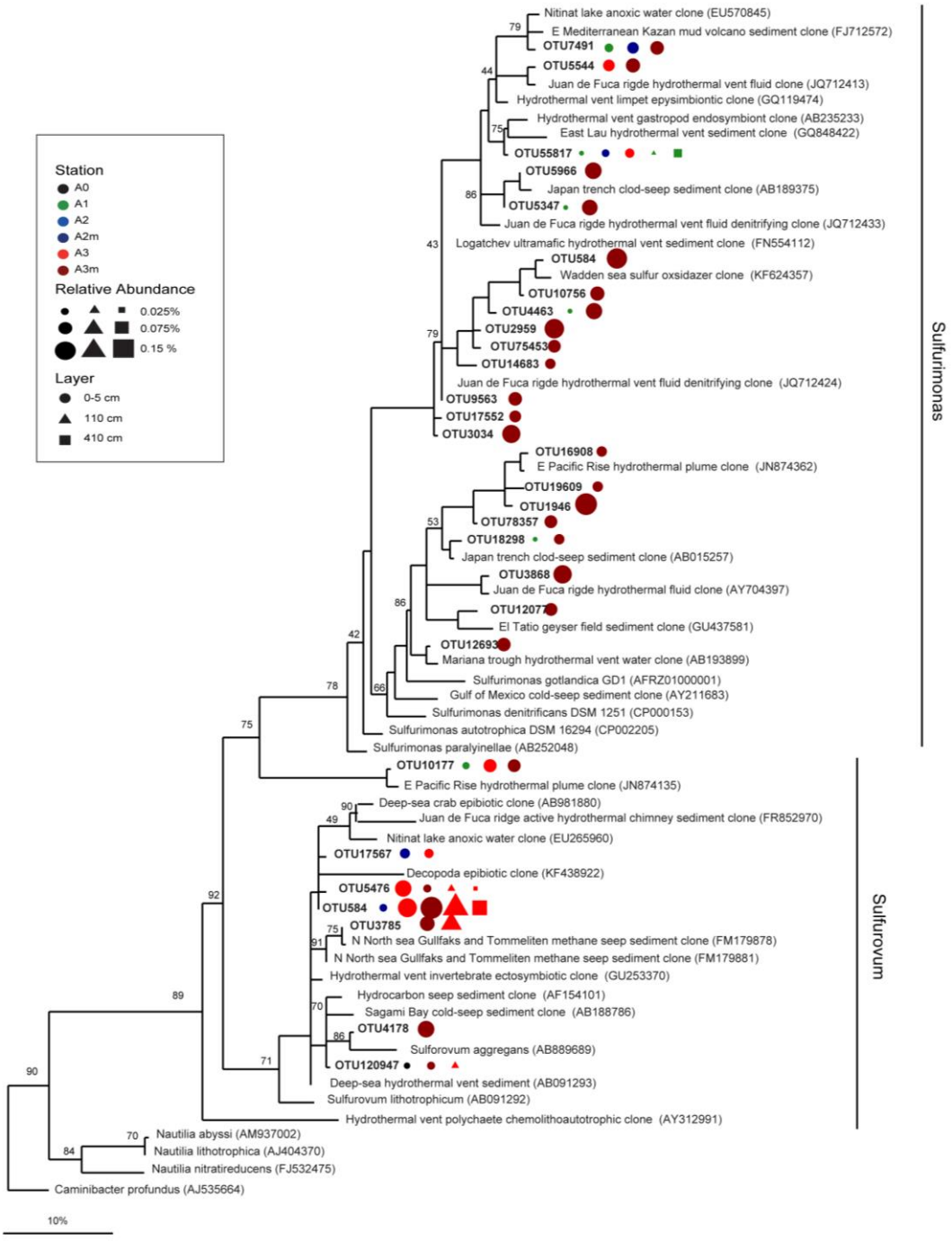

Figure 4.11. Phylogenetic tree of the family Helicobacteraceae. The tree backbone was constructed, including only the reference sequences, with Maximum Likelihood Method and 500 bootstraps were performed; then SWIR Helicobacteraceae sequences were added with Parsimony Method. SWIR Helicobacteraceae sequences are bolded.

Figure 4.14. Phylogenetic tree of the archaeal family DHVEG-6. The tree backbone was constructed, including only the reference sequences, with Maximum Likelihood Method and 500 bootstraps were performed; then SWIR DHVEG-6 sequences were added with Parsimony Method. SWIR DHVEG-6 sequences are bolded.

(next page) ▶

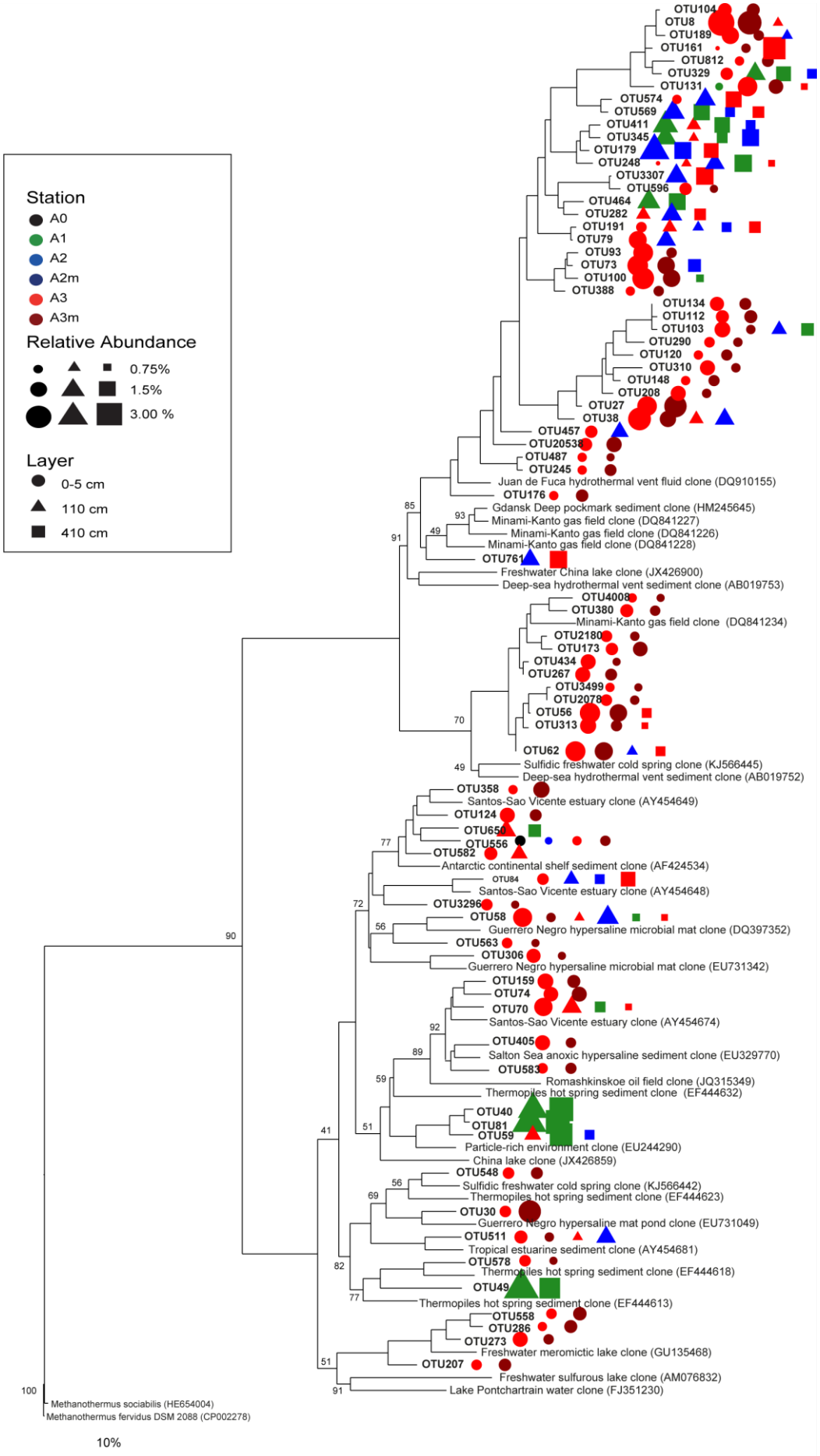
Station
A0
A1
A2
A2m
A3
A3m
Relative Abundance
0.75%
1.5%
3.00 %
Layer
0-5 cm
110 cm
410 cm
OTU104
OTU8
OTU189
OTU161
OTU812
OTU329
OTU131
OTU574
OTU569
OTU411
OTU345
OTU179
OTU248
OTU3307
OTU596
OTU464
OTU282
OTU191
OTU79
OTU93
OTU73
OTU100
OTU388
OTU134
OTU112
OTU103
OTU290
OTU120
OTU310
OTU148
OTU208
OTU27
OTU38
OTU457
OTU20538
OTU487
OTU245
Juan de Fuca hydrothermal vent fluid clone (DQ910155)
OTU176
Gdansk Deep pockmark sediment clone (HM245645)
Minami-Kanto gas field clone (DQ841227)
Minami-Kanto gas field clone (DQ841226)
Minami-Kanto gas field clone (DQ841228)
OTU761
Freshwater China lake clone (JX426900)
Deep-sea hydrothermal vent sediment clone (AB019753)
OTU4008
OTU380
Minami-Kanto gas field clone (DQ841234)
OTU2180
OTU173
OTU434
OTU267
OTU3499
OTU2078
OTU56
OTU313
OTU62
Sulfidic freshwater cold spring clone (KJ566445)
Deep-sea hydrothermal vent sediment clone (AB019752)
OTU358
Santos-Sao Vicente estuary clone (AY454649)
OTU124
OTU650
OTU556
OTU582
Antarctic continental shelf sediment clone (AF424534)
OTU84
Santos-Sao Vicente estuary clone (AY454648)
OTU3296
OTU58
Guerrero Negro hypersaline microbial mat clone (DQ397352)
OTU563
OTU306
Guerrero Negro hypersaline microbial mat clone (EU731342)
OTU159
OTU74
OTU70
Santos-Sao Vicente estuary clone (AY454674)
OTU405
Salton Sea anoxic hypersaline sediment clone (EU329770)
OTU583
Romashkinskoe oil field clone (JQ315349)
Thermopiles hot spring sediment clone (EF444632)
OTU40
OTU81
OTU59
Particle-rich environment clone (EU244290)
China lake clone (JX426859)
OTU548
Sulfidic freshwater cold spring clone (KJ566442)
Thermopiles hot spring sediment clone (EF444623)
OTU30
Guerrero Negro hypersaline mat pond clone (EU731049)
OTU511
Tropical estuarine sediment clone (AY454681)
OTU578
Thermopiles hot spring sediment clone (EF444618)
OTU49
Thermopiles hot spring sediment clone (EF444613)
OTU558
OTU286
OTU273
Freshwater meromictic lake clone (GU135468)
OTU207
Freshwater sulfurous lake clone (AM076832)
Lake Pontchartrain water clone (FJ351230)
Methanothermus sociabilis (HE654004)
Methanothermus fervidus DSM 2088 (CP002278)
10%

5. Discussion

The segment 10°-16°E of South West Indian Ridge (SWIR), with a spreading speed of only 8 mm/year, is the slowest segment of any other spreading ridge (Dick et al. 2003). Despite the low spreading rate and the reduced magma input, Bach et al. (2002) measured temperature and turbidity anomalies in bottom water of this SWIR section, suggesting the presence of hydrothermal emissions. To confirm the presence of hydrothermal circulation, in 2013 the expedition ANTXXIX/8 was carried out employing seismology, geology, microbiology, heat flow analyses and others. The presence of hydrothermal plume in bottom water was not confirmed and it has not been observed water/gas emissions at seafloor. However, anomalies in heat flow, typically a signature of magma upwelling, and pore water biogeochemistry and also the recovery of organisms related to fauna vents suggested the existence of some type of hydrothermal circulation at SWIR. The results of this intensive survey allowed to identify three areas with different properties: Area 1 (A1) with higher heat flux below the seafloor; Area 2 (A2) where in 2002 it was hypothesized the presence of hydrothermal emissions (Bach et al., 2002), but not confirmed by expedition ANTXXIX/8; Area 3 (A3) with anomalies of methane, ammonium, sulphide and dissolved inorganic carbon (DIC) in pore water sediment profiles, and recovery of fauna vents (i.e. Vesicomyid clam and tube worm Pogonophora).

The hypothesis of my thesis is that the presence of hydrothermal fluxes, changing the sediment geochemistry, is responsible of benthic microbial community modification. In particular, the biogeochemistry observed in this A3 could support chemolithoautotrophic prokaryotes and specific microbial consortia. To test this hypothesis I analyzed sediment samples collected in three SWIR's areas (A1, A2

and A3) and in a reference area (A0), located outside and south to the ridge. In order to assess differences in benthic prokaryotic assemblage between areas, Illumina 16S gene tag sequencing was applied to describe bacterial and archaeal diversity and community structure. Statistical tools were used to highlight differences amongst areas and identify prokaryotic taxa responsible for these differences. Furthermore, with the construction of phylogeny trees, I investigated relationship between the OTUs identified in this study and Bacteria and Archaea found in deep-sea chemosynthetic environments (e.g. hydrothermal vents, cold seeps, hydrate-bearing sediments, mud volcanos).

The comparison of bacterial and archaeal community structure showed that A3 held a different prokaryotic community compared to other SWIR's areas (mostly for Bacteria) and reference area, both Bacteria and Archaea (Figure 4.1; Figure 4.12). In particular it is relevant that Bacteria, representing the dominant prokaryotic domain in all stations investigated (relative abundance higher than 70%; data not shown), showed a community composition very different to those observed in other areas (up to 70% of dissimilarity). The presence of specific bacterial and archaeal communities in A3 was also supported by analysis of beta-diversity (i.e. OTUs turnover). The A3 shared less OTUs with A2 than those shared between A2 and A1, despite A2 was closer to A3 than A1 (Figure 4.2). Even the reference area, which was about equally distant from all the SWIR areas, shared more OTUs with A1 and A2 than with A3. Thus prokaryotic taxa turnover at A3 did not show a typical distant-decay relationship, as expected for deep-sea surface sediments (Zinger et al., 2014). Indeed under homogenous environmental setting and not isolate ecosystems (e.g. without physical or biogeochemical barriers), the similarity in taxonomic composition of biological

assemblages decreases with increasing of geographic distances (Nekola and White, 1999). Conversely taxa turnover at A3 is similar to those describe for microbial communities at hydrothermal/seep environments, where, due to the presence of biogeochemical barriers, the microbial assemblages are isolated from other environments, sharing with them lowest number of taxa (Zinger et al., 2011; Ruff et al., 2014). Also the alfa-diversity suggests the presence of hydrothermal related bacterial and archaeal communities at A3. Both bacterial and archaeal OTUs estimated richness were lower at A3 than at other areas. The decrease of diversity and increase of endemism is expected in presence of hydrothermal/seep fluxes, which, leading a supply of chemical energy sources and a highly reduced environment, favours the development of a microbial community dominated by specialised taxa (Leibold et al., 2004; Ruff et al, 2014). The higher bacterial diversity and the increase of rare biosphere observed in other SWIR and reference areas align with what previously findings for the deep-sea environment (Sogin et al., 2006).

The bacterial and archaeal communities in subsurface layers investigated, 110 cm and 410 cm below seafloor (bsf), were weakly area specific (Figure 4.3; Figure 4.4; Figure 4.13) and they did not show substantial differences in alpha-diversity (Table 4.1; Table 4.2). A reason could be that, in general, the subsurface sedimentary compartment is more homogenous than the surface habitat (Takai et al., 2004). Unfortunately the lack of reference samples for these layers makes not possible to assess if the similarity between SWIR areas may be due or not to a hydrothermal circulation effect on subsurface environment along all rift valley. Analysing bacterial beta-diversity along vertical sediments profiles, I observed that at A3 the subsurface layers shared a higher numbers of OTUs with surficial

layer compared to what saw at A2 and A3. Furthermore at A3 the surficial and subsurface bacterial communities were more similar to each other than at A2 and A1 (Figure 4.2c). Since the differentiation of microbial community with sediment depth is mainly driven by sediment burial and aging (Durbin and Teske, 2011), the higher beta-diversity and similarity of bacterial communities observed at A3 can be due to the presence of hydrothermal circulation, which promotes exchanges between surface and subsurface environments.

Some of dominant bacterial and archaeal classes identified in area 3 are typically described also for deep-sea hydrothermal and seep systems, and these are Deltaproteobacteria and JS1 for Bacteria, and Halobacteria and Thermoplasmata for Archaea (Anderson et al., 2015; Ruff et al., 2015; Webster *et al*., 2004; Harrison *et al*., 2009). Conversely the reference area is dominated by deep-sea benthic taxa, such as Gammaproteobacteria, Alphaproteobacteria, Acidomicrobiia and Planctomycetacia (Figure 4.3). Interesting A0 showed a bacterial community composition similar to that described by Ruff and colleagues (2014) for station located in Antarctic Polar Front, at northeast of the SWIR (52,011 °S; 10,011 °E). This station was characterized by thick diatom ooze, which was also observed in SWIR stations. The presence of this diatom ooze in deep-sea sediments is typical for the Antarctic Polar Front, whereas it did not occur south of SWIR, where the reference area (A0) was located, which sediment is dominated by siliciclastic clay (Dutkiewicz et al. 2015). Despite the areas outside the SWIR have different sedimentary properties (i.e. sediment composition and porosity), bacterial communities were more similar than the communities between the northern site and A3, even if, here, the sediment had the same composition. For example, Rhodospirillaceae, Rhodobacteraceae,

Sh766B-TzT-29, Planctomycetaceae, Phycisphaeraceae and Acidobacteraceae are taxa that in both the reference sites compose the majority of the bacterial dominant community and they are barely represented in A3.

The highest bacterial sequences phylogenetically related to bacteria isolated in hydrothermal and seep environments were found in Area 3, reaching 40-43% of dominant community (defined here as those OTUs that are present with more than one sequence in the whole dataset). Furthermore the percentage decreased with the distance from A3, with lowest value at reference area (<5%; Figure 5.1). The same trend was observed in archaea dominant community: in A3 the community was constituted for 40-70% by sequences related to Archaea found in deep-sea hydrothermal vents and seeps. In the reference area, only 2% of archaeal sequences were associated with seep and hydrothermal isolated (Figure 5.2). At studied areas, the potential chemolithoautotrophic organisms constituted a minor part of the dominant bacterial and archaeal communities. In fact, it represented about 6% of all the sequences; 4% of which was found in A3 (Figure 5.1). I decided not to include ammonia oxidizing organisms in this estimate, like bacterial Nitrosomonas and archaeal Nitrosopumilus, since the oxidation of ammonia is a process not related only to hydrothermalism, as the ammonia is a product of organic matter degradation, and these taxa are ubiquitous in marine sediments (Vannelli et al., 1990; Walker et al., 2010). In my dataset the chemolithoautotrophic community was composed by bacteria belonging to Epsilonproteobacteria, Acidoferribacterales, Sar406 and VC2.1 Bac22. The phylum Epsilonbacteria is usually dominant in hydrothermal systems (Nakagawa et al., 2005). The found genera are Sulfurovum, Sulfurimonas and Arcobacter, which are classified as sulphur oxidizers (Nunoura et al., 2012).

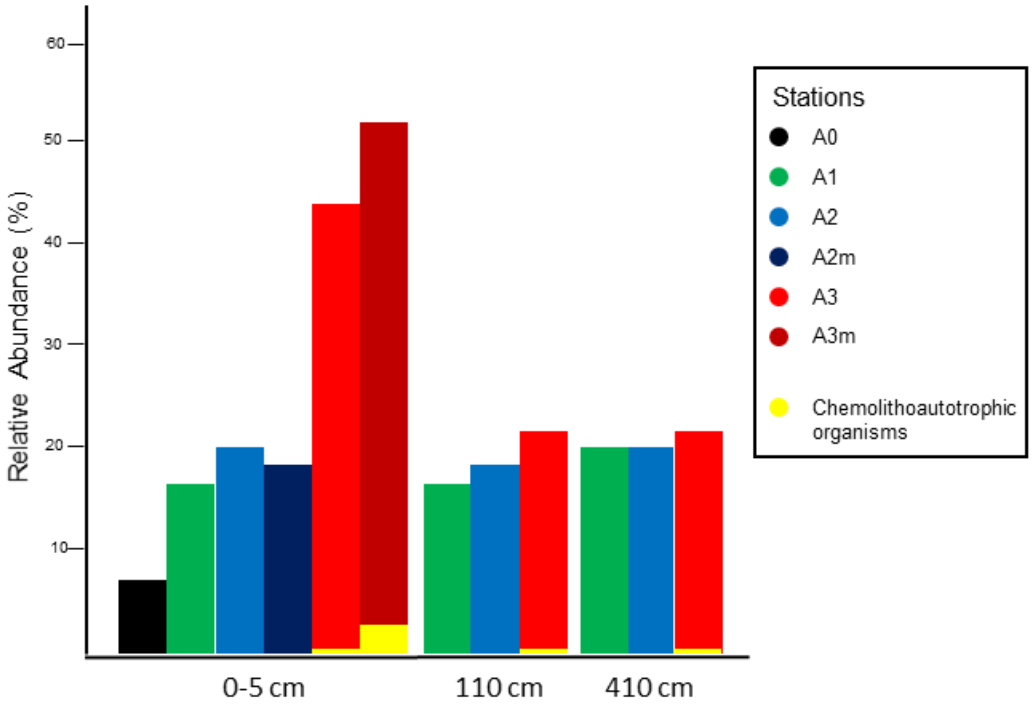

Figure 5.1. Histogram showing the relative abundance of bacterial sequences close related to hydrothermal –driven systems. The sequences close related to chemolithoautotrophic bacterial clones are in yellow.

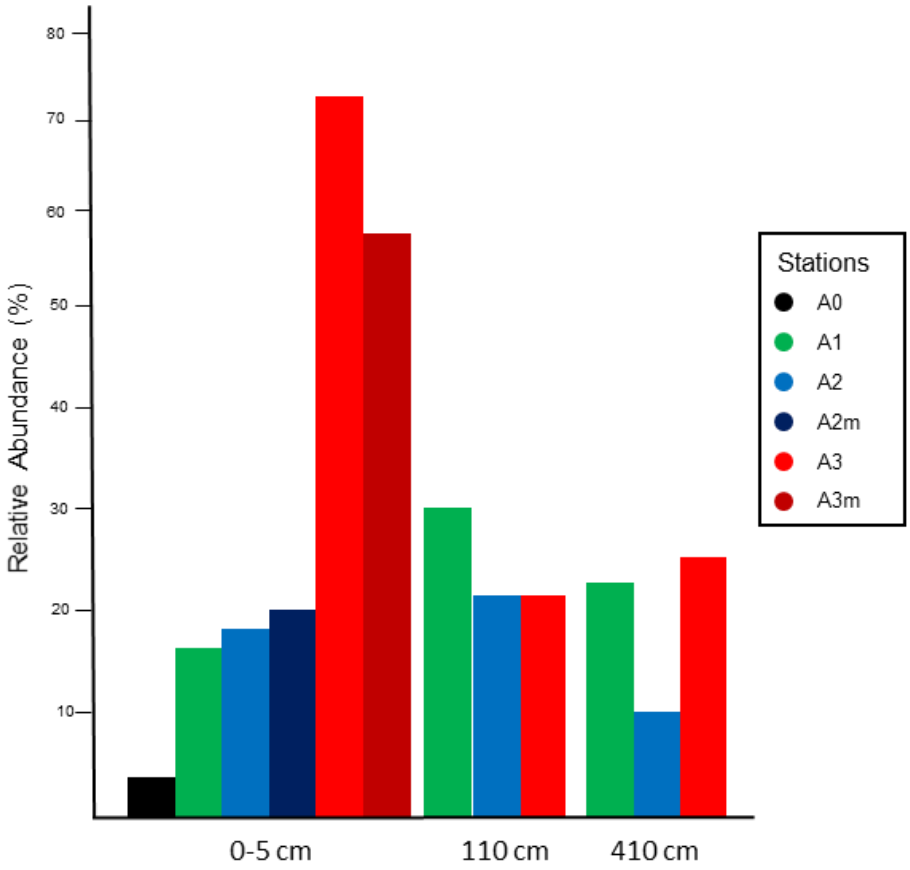

Figure 5.2. Histogram showing the relative abundance of archaeal sequences close related to hydrothermal –driven systems.

Another potential sulphur oxidizers belonged to Acidoferribacterales (Hallberg, 2011), which was also identify in A3. Interesting, the higher sulphide concentrations in A3 pore water than in other investigated areas supports the presence of these chemolithotrophs.

Other two taxa that showed phylogenetic related with chemolithoautotrophic were Sar406 and Vc2.1 Bac22 (Figure 4.9; Figure 4.10). Sar406 is particularly abundant in oxygen depleted environments and supposed to have a sulfur-based energy metabolism (i.e. dissimilatory sulphur oxidation; Wright et al., 2014), whereas Va2.1bac22 has been found manly in hydrothermal plume (Meyer et al.2013) and as endosymbiont of hydrothermal fauna (Alain et al. 2012).

The low contribution of chemolithotrophs is the main difference with prokaryotic communities described so far for many deep-sea hydrothermal vents (Tyler et al., 2003). However, the composition of hydrothermal fluids can be very different (German and Seyfried, 2014) and therefore give rise to different communities of chemolithotrophs (Boetius, 2005; Dick et al., 2013). The well investigated fast and slow spreading ridges showed that vent-fluid compositions depend on lithospheric substrate, with which hydrothermal fluids interact, and on origin of heat (i.e. magmatism vs tectonism; German and Seyfried, 2014). At one extreme there are the black-smokers in basal systems with a hydrothermal circulation generated by magma upwelling and with acid (pH 3 to 5) and high temperature (200°C to 400 °C) fluids enriched in CO_2 and sulphide, which are inhabited mostly by acidophilic, hyperthermophilic sulphite oxidizers (Boetius, 2005). At the other extreme there are the white-smokers in ultramafic systems fuelled by tectonism (i.e. serpentinization reactions), which, providing high fluxes of hydrogen and methane at warm temperatures and high pH, sustains hydrogen and methane

oxidizing communities (Kelly et al., 2005; Kelly et al., 2007). The ultraslow spreading ridges began to be explored only 15 years ago, and if little is known about the origin of hydrothermal circulation, venting properties and fluids compositions (Snow and Edmonds, 2007; German et al., 2010), the knowledge of microbial diversity is practically absent (Peng et al. 2011). However one important peculiarity of ultraslow speeding ridges is thin crust thickness (<1 km; Dick et al., 2001). The lack of ocean crust allows to deep seawater to more easily reach the mantle, which loss of heat can contribute and interplay with tectonic on the formation and evolution of hydrothermal circulation even when magma supply is limited. The presence of geochemical anomalies in axial region of SWIR, the lack of abundant vent fauna and chemolithotrophs, here observed, could support the presence of widespread low temperature diffuse fluid leakage generated by loss of heat from the mantle.

Although the other chemosynthetic environment related taxa were not classified like autotrophic prokaryotes, some of them are key taxa in support of my hypothesis, since they are partners of consortia and/or mediate specific reaction (e.g. hydrocarbon degradation) typically described for hydrothermal and seep environments. SEEP-srb1 is a heterotrophic sulphate reducing (SR) organism mainly found in seep systems. This taxon usually forms specific consortia with ANME-2, a methanotrophic archaea, in hydrothermal and seep systems (Orcutt et al., 2010; Orphan et al. 2010). To these consortia is attributable the anaerobic oxidation of methane (AOM). ANME archaea oxidase methane and transfer the obtained electron to SR bacteria through an unknown mechanism (Schreiber et al. 2010); the electron is used by SR bacteria to reduce sulphate to sulphide. Despite the methane anomalies found at A3 could support the presence of these

consortia, in the dataset, I didn't find the archaeal partner (ANME-2) that usually forms consortia with SEEP-sbr1. The lack of ANME-2 could be ascribed to methodological problems like the non-specificity of the primers used (Ding et al.,2015) or the DNA extraction procedure or the low amount of archaeal DNA. Another problem could be the lack of knowledge about metabolism of uncultivated archaea, indeed in my dataset several archaea taxa were found mainly at A3 but for which metabolism is unknown (Takano et al., 2010).

In the dataset I found two other SR bacteria belonging to the phylum Deltaproteobacteria: Desulfarculaceae and WCHB1-69. These bacterial families are not exclusive of seep systems (Kuever, 2014; Okabe et al., 2003), however the OTUs here found were phylogenetically close to seep bacterial clones. In the work of McGlynn et al. (2015) consortia between ANME and organisms belonging to the phylum Deltaproteobacteria were described.

The high relative abundance of sulphate reducer organisms observed in A3 has to be also related to differences in quality and availability of sedimentary organic matter, since these organisms are specialized in exploiting labile organic substrates for their growth (Hao et al., 1996). Thus, they are typically abundant in anaerobic sediments with large amount and fresh organic matter as costal sediments and chemoshinthetic habitats (Muyzer and Stams, 2008). Conversely deep-sea sediments, due to high oxygen penetration, low food supply and large fraction of refractory organic matter, are not the ideal habitat for sulphate reducing bacteria (Jørgensen and Boetius, 2007). Furthermore, hydrothermal circulation can lead to removal of recalcitrant dissolved organic molecules and to increased concentrations of small organic compounds such as formate, acetate, methanol, methanethiol and amino acids, and mixtures of hydrocarbon (Hawkes et al.,

2015), favouring therefore specific heterotrophic microbes. According to this, I found in A3 several bacterial taxa involved in degradation of these organic compounds under sulphate reducing condition: Spirochaeteacea and Anaerolinaceae are involved in the fermentation and oxidation of alkanes (Liang et al. 2015); the sequences of OP8, mostly recovered in subsurface layer, have been found related to bacteria isolated from marine sediments rich in hydrocarbons (Figure 4.6).

Finally, the archaea taxon Deep Sea Hydrothermal Vent Group 6 (DHVEG 6) represented more than 50% of the dominant archaeal community in A3. Despite this archaeal family is ubiquitous (Nonoura et al., 2011; Xie et al., 2014), the SWIR sequences clustered chiefly close to hydrothermal clones (Figure 4.14). The new phylogenetic tree shows as the OTUs, previously ascribed to DHVEG 6, are now clustered into two different phyla: Pacearchaeaota and Woesearchaeota. The approach applied by Castelle and colleagues (2015) allows also to better elucidate the potential metabolism of these archaeal phyla. OTUs belonging to Pacearchaeaota clustered close to the reference sequence AR13, which is supposed to have a saccharolytic and fermentative lifestyle. Instead, sequences belonging to Woesearchaeota were located between organisms AR11 and AR20, which have a carbon and hydrogen metabolism probably associated with symbiotic and/or fermentation-based lifestyles (Figure 5.3). Thus, as discussed above for sulphate reducers, the presence of microorganisms with hydrogen and fermentative related metabolism is expected in anaerobic and organic matter rich sediments typical for seep and hydrothermal systems and not for deep-sea floor.

Figure 5.3. Phylogenetic tree of the archaeal superphylum DPANN. The tree backbone was constructed, including only the reference sequences, with Maximum Likelihood Method and 500 bootstraps were performed; then SWIR VC2.1 DHVEG-6 sequences were added with Parsimony Method. SWIR DHVEG-6 sequences are bolded.

(next page)

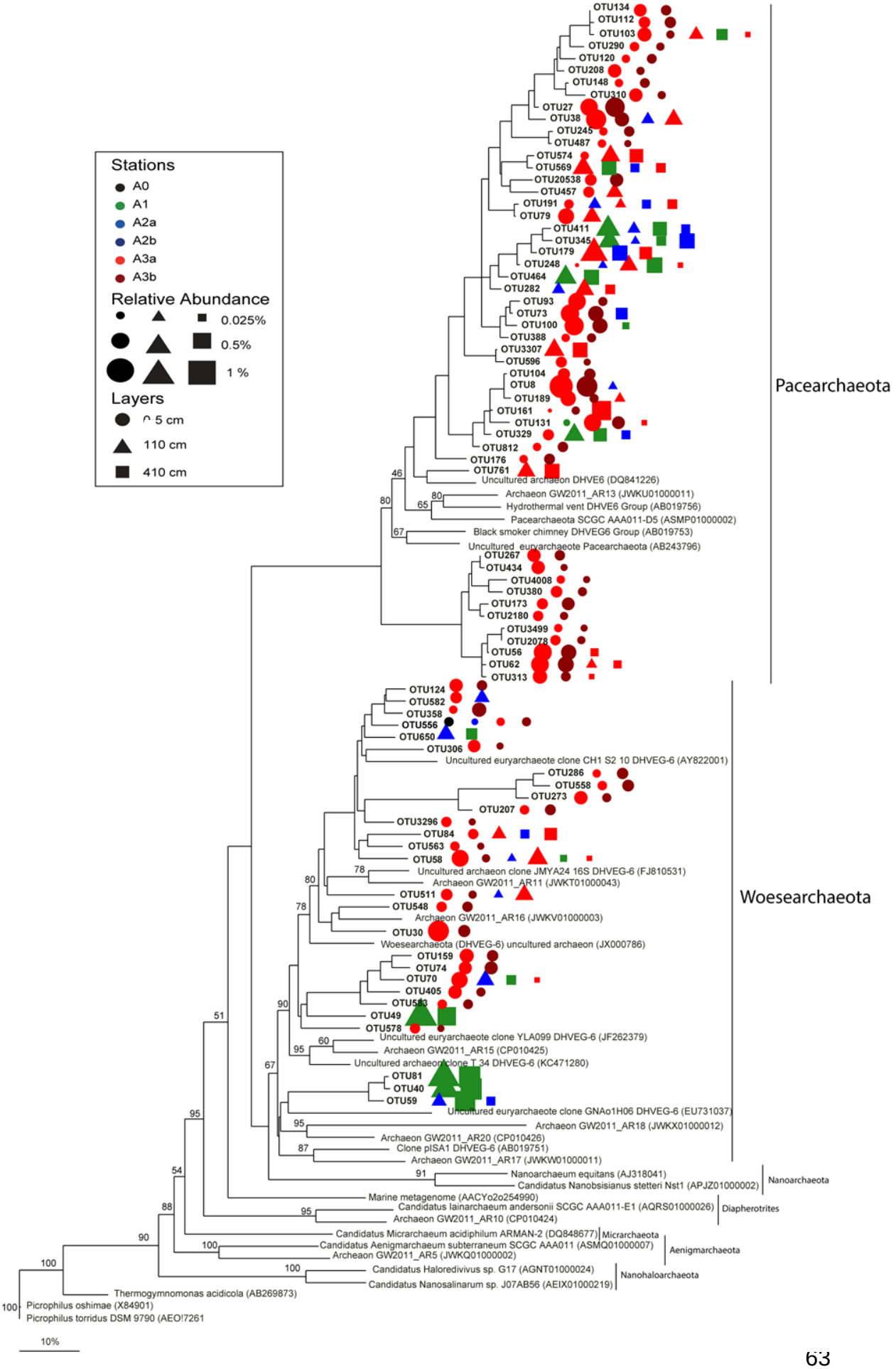
Stations
A0
A1
A2a
A2b
A3a
A3b
Relative Abundance
0.025%
0.5%
1 %
Layers
0.5 cm
110 cm
410 cm
OTU134
OTU112
OTU103
OTU290
OTU120
OTU208
OTU148
OTU310
OTU27
OTU38
OTU245
OTU487
OTU574
OTU569
OTU20538
OTU457
OTU191
OTU79
OTU411
OTU345
OTU179
OTU248
OTU464
OTU282
OTU93
OTU73
OTU100
OTU388
OTU3307
OTU596
OTU104
OTU8
OTU189
OTU161
OTU131
OTU329
OTU812
OTU176
OTU761
Uncultured archaeon DHVE6 (DQ841226)
Archaeon GW2011_AR13 (JWKU01000011)
Hydrothermal vent DHVE6 Group (AB019756)
Pacearchaeota SCGC AAA011-D5 (ASMP01000002)
Black smoker chimney DHVEG6 Group (AB019753)
Uncultured euryarchaeote Pacearchaeota (AB243796)
Pacearchaeota
OTU267
OTU434
OTU4008
OTU380
OTU173
OTU2180
OTU3499
OTU2078
OTU56
OTU62
OTU313
OTU124
OTU582
OTU358
OTU556
OTU650
OTU306
Uncultured euryarchaeote clone CH1 S2 10 DHVEG-6 (AY822001)
OTU286
OTU558
OTU273
OTU207
OTU3296
OTU84
OTU563
OTU58
Uncultured archaeon clone JMYA24 16S DHVEG-6 (FJ810531)
Archaeon GW2011_AR11 (JWKT01000043)
OTU511
OTU548
Archaeon GW2011_AR16 (JWKV01000003)
OTU30
Woesearchaeota (DHVEG-6) uncultured archaeon (JX000786)
OTU159
OTU74
OTU70
OTU405
OTU583
OTU49
OTU578
Uncultured euryarchaeote clone YLA099 DHVEG-6 (JF262379)
Archaeon GW2011_AR15 (CP010425)
Uncultured archaeon clone T 34 DHVEG-6 (KC471280)
OTU81
OTU40
OTU59
Uncultured euryarchaeote clone GNAo1H06 DHVEG-6 (EU731037)
Archaeon GW2011_AR18 (JWKX01000012)
Archaeon GW2011_AR20 (CP010426)
Clone pISA1 DHVEG-6 (AB019751)
Archaeon GW2011_AR17 (JWKW01000011)
Woesearchaeota
Nanoarchaeum equitans (AJ318041)
Candidatus Nanobsisianus stetteri Nst1 (APJZ01000002)
Nanoarchaeota
Marine metagenome (AACYo2o254990)
Candidatus Iainarchaeum andersonii SCGC AAA011-E1 (AQRS01000026)
Archaeon GW2011_AR10 (CP010424)
Diapherotrites
Candidatus Micrarchaeum acidiphilum ARMAN-2 (DQ848677)
Candidatus Aenigmarchaeum subterraneum SCGC AAA011 (ASMQ01000007)
Archeaon GW2011_AR5 (JWKQ01000002)
Micrarchaeota
Aenigmarchaeota
Candidatus Haloredivivus sp. G17 (AGNT01000024)
Candidatus Nanosalinarum sp. J07AB56 (AEIX01000219)
Nanohaloarchaeota
Thermogymnomonas acidicola (AB269873)
Picrophilus oshimae (X84901)
Picrophilus torridus DSM 9790 (AEO!7261
10%

6. Conclusions

The results of this study on bacterial and archaeal communities at SWIR and reference areas showed that the diversity and community composition of benthic prokaryotic assemblages found in Area 3, where the geochemical profiles suggest the presence of hydrothermal fluxes, were more similar to those described for seep and hydrothermal vent habitats than to those of deep-sea floor.

To date only few black-smoker-like hydrothermal emissions were described for ultraslow spreading ridge (Sohn et al., 2008; Tao et al., 2012), thus the presence of hydrothermal microbial communities in ultraslow ridge fragments not interested by intense hydrothermalism has important implication in understanding the functioning of ultraslow ridges and their role in global biogeochemical cycles and vent organisms dispersion. The ultraslow spreading system is about 1/4 of global divergent plate boundaries (Snow and Edmonds, 2007), so widespread emissions on large portion of rift valley seafloor, so far neglected, could contribute to the loss of heat and to the global geochemical budgets like or more than faster (smokers-hosted) ridges. Furthermore, the SWIR, connecting faster classes of ridges located in Indian, Atlantic and Pacific Oceans, has also an important role in dispersion of for hydrothermal vent fauna (Germal et al., 1998; Van Dover CL et al., 2002). Despite the distributed emissions along fragment of SWIR could not support large community of vents fauna, they can facilitate the vent larval dispersion, offering a suitable environment between hot spots of hydrothermalism (e.g. black-smokers).

7. Supplementary materials

7.1 Figures

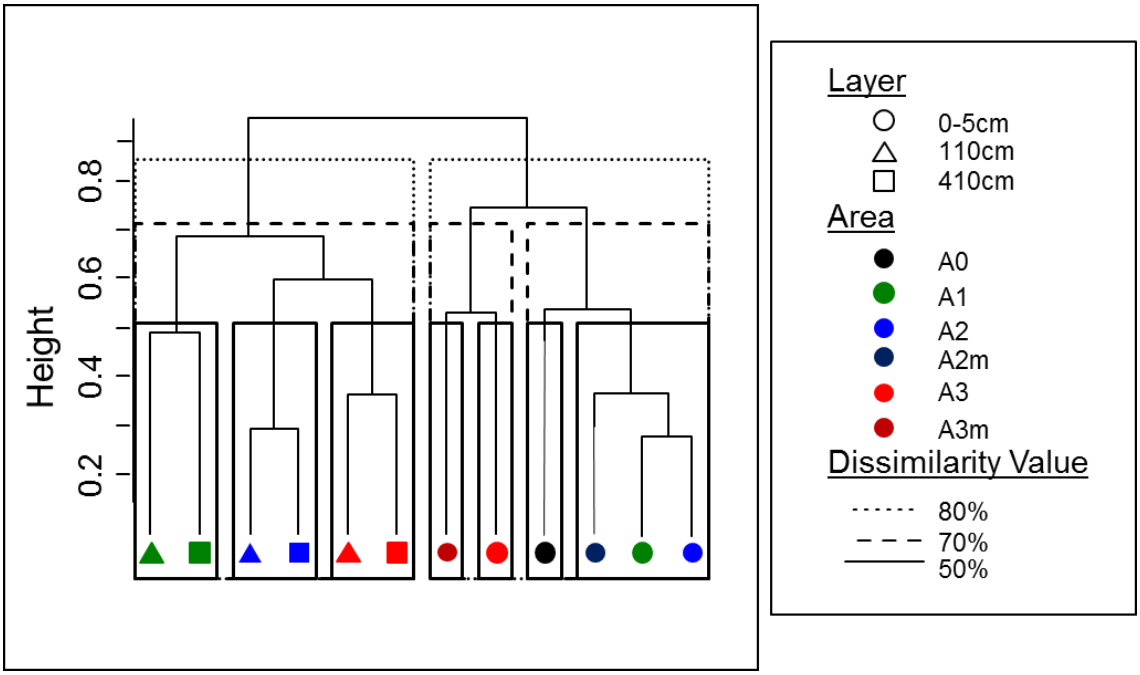

Figure S1. Cluster analysis performed with average method on OTUs bacterial relative abundances.

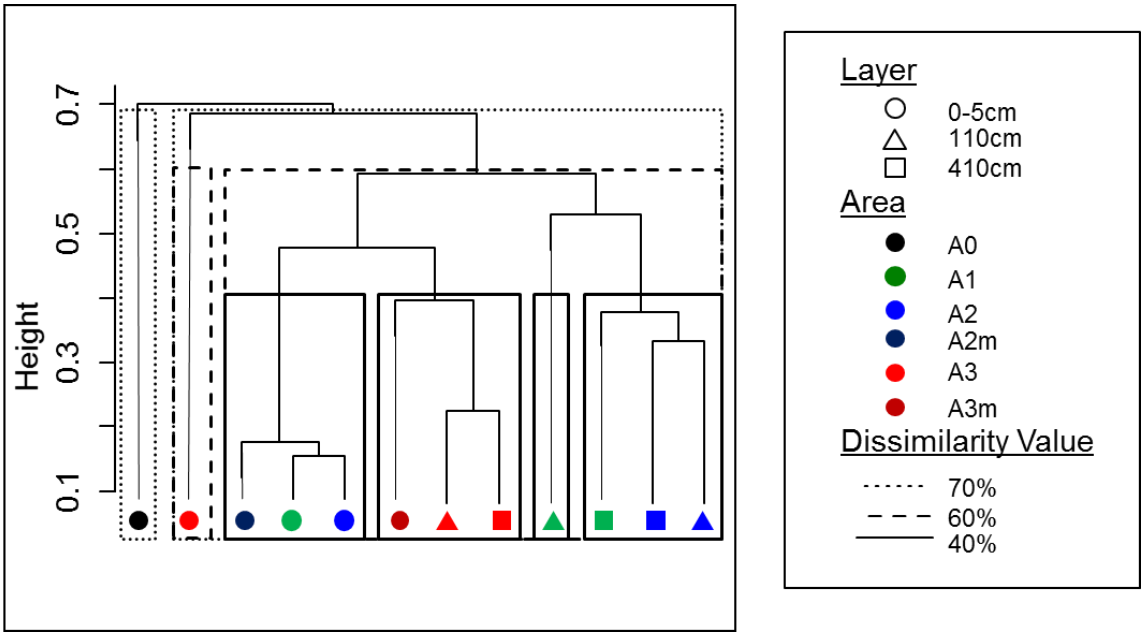

Figure S2. Cluster analysis performed with average method on the OTUs archaeal relative abundances.

a

Sample	Layer	Extraction 1		Extraction 2		Final Sample	
		DNA Conc	DNA Am	DNA Conc	DNA Am	DNA Conc*	DNA Am
	cm	ng/ml	ug	ng/ul	ug	ng/ul	ug
A0	0-1	16.1	1.5	23.4	2.1		
A0	1-5	23.0	2.1	21.3	1.9	21.0	7.6
A3m	0-1	24.8	2.2	8.6	0.8		
A3m	1-5	10.4	0.9	13.4	1.2	10.7	3.9
A2m	0-1	15.4	1.4	11.1	1.0		
A2m	1-5	19.8	1.8	25.7	2.3	18.1	6.5
A1	0-1	23.0	2.1	22.0	2.0		
A1	1-5	21.8	2.0	21.2	1.9	22.3	8.0
A2	0-1	32.8	3.0	20.5	1.8		
A2	1-5	19.2	1.7	21.4	1.9	23.0	8.3
A3	0-1	8.4	0.8	8.2	0.7		
A3	1-5	10.3	0.9	9.3	0.8	9.3	3.3

b

Sample	Layer	Extraction 1		Extraction 2		Precipitation 1		Extraction 3		Extraction 4		Precipitation 2		Final Sample	
		DNA Conc	DNA Am	DNA Conc	DNA Am	DNA Conc	DNA Am	DNA Conc	DNA Am	DNA Conc	DNA Am	DNA Conc	DNA Am	DNA Conc	DNA Am
	cm	ng/ml	ug	ng/ml	ug	ng/ml	ug	ng/ml	ug	ng/ml	ug	ng/ml	ug	ng/ul	ug
A1_2**	110	6.7	0.6	7.8	0.7	17.3	0.5	6.3	0.6	5.3	0.5	10.1	0.3	10.7	0.5
A1_2**	410	6.3	0.6	9.7	0.9	21.7	0.7	8.4	0.8	10.5	0.9	16.5	0.5	17.3	0.9
A1	110	8.0	0.7	9.0	0.8	18.4	0.6	10.1	0.9	6.8	0.6	17.8	0.5	16.1	0.8
A1	410	10.0	0.9	12.7	1.1	24.1	0.7	10.2	0.9	12.3	1.1	17.6	0.5	18.1	0.9
A2	110	9.1	0.8	9.5	0.9	28.2	0.8	9.3	0.8	9.4	0.8	16.8	0.5	18.2	0.9
A2	410	7.9	0.7	9.9	0.9	23.1	0.7	7.9	0.7	8.9	0.8	12.2	0.4	16.9	0.8
A3	110	6.9	0.6	11.1	1.0	33.2	1.0	8.8	0.8	8.8	0.8	11.6	0.3	16.9	0.8
A3	410	9.7	0.9	12.6	1.1	29.0	0.9	12.1	1.1	11.4	1.0	14.0	0.4	18.8	0.9

Table S1. Extractions and precipitations performed on DNA a) surface samples and b) subsurface samples. DNA Conc, DNA Concentration; DNA Am, DNA Amount. *DNA concentrations after the combination of the surface layer samples; **discarded samples. After each extraction DNA was suspended in 90 ul of PCR water; after each precipitation it was suspended in 30 ul of TE. The final volume was 360 ul for surface samples and 50 ul for subsurface samples.

OTU	A1 vs A3 (%)	A2 vs A3 (%)	A1 vs A2 (%)	Taxa
otu2	4.62	4.24	1.71	Candidate division OP8
otu3	4.30	4.78	0.79	Candidate division JS1
otu5	3.61	1.65	2.99	Candidate division OP8
otu7	2.05		2.63	Sh765B-AG-111
otu1	1.67	4.74	6.85	Candidate division JS1
otu12	1.39	1.04	0.75	Candidate division OP8
otu4	1.33	0.91	2.16	Candidate division JS1
otu17	1.24	1.12	0.48	Candidate division KB1
otu21	1.16	1.31		Candidate division JS1
otu8	1.12	0.83	1.45	Ralstonia
otu31	1.10		1.41	Candidate division OP8
otu11	0.96	1.51	0.79	Candidate division JS1
otu20	0.91	1.10		BD2-2
otu6	0.87			Hyphomicrobiaceae
otu55	0.79	0.99		Dehalococcoidia
otu23	0.71	0.67	0.54	Candidate division KB1
otu40	0.70	0.33	0.64	Anaerolineales
otu68	0.69	0.47	0.41	Anaerolineaceae
otu45	0.67			Napoli-4B-65
otu54	0.66		0.70	Candidate division OP8
otu125	0.65			Dehalococcoidia
otu9	0.64	1.28	0.45	Candidate division JS1
otu27	0.64			MSB-5B2
otu119	0.63		0.79	Candidate division JS1
otu37	0.56	0.56	0.64	Candidate division OP8
otu14	0.53	1.12	0.68	Candidate division OP8
otu16	0.52		0.46	GIF3
otu70	0.52			BHI80-139
otu52	0.51	0.61		BHI80-139
otu429	0.51		0.65	NPL-UPA2
otu24	0.49	0.63		Napoli-4B-65
otu36	0.48		0.60	Sh765B-AG-111
otu50	0.47	0.34		Desulfarculales
otu26	0.44	0.48	0.42	Anaerolineaceae
otu76	0.44	0.33	0.57	Alicyclobacillus
otu77	0.41	0.51		Candidate division KB1
otu107	0.40			Candidate division OP8
otu44	0.39	0.45		Rhodospirillaceae
otu78	0.37	0.45		Candidate division JS1
otu61	0.37		0.47	vadinBA26
otu33	0.36	0.29	0.46	Alicyclobacillus
otu226	0.36		0.30	SAR406 clade(Marine group A)
otu65	0.35			Anaerolineaceae
otu87	0.35		0.45	Candidate division OP8
otu121	0.35		0.45	Sh765B-AG-111
otu143	0.33	0.34		Spirochaetes
otu29	0.32		0.36	MSBL2
otu48	0.32			Candidate division JS1
otu529	0.31		0.31	TA06
otu81	0.31	0.40		Candidate division OD1
otu94	0.30	0.38		Dehalococcoidia
otu139	0.29		0.38	Candidate division OP8
otu376	0.29		0.37	NPL-UPA2
otu105	0.28	0.35		GIF3
otu102		0.30		Candidate division OD1
otu238		0.30		MSBL5
otu13		1.50	1.16	MSBL5
otu19		1.36	1.22	Candidate division OP8
otu15		1.18	1.19	Candidate division OP8
otu16		1.14		GIF3
otu6		0.94	0.31	Hyphomicrobiaceae
otu63		0.70	0.61	Dehalococcoidia
otu41		0.67	0.46	Candidate division OP8
otu62		0.50	0.46	S085
otu69		0.38		FW22
otu160		0.37		CCM11a
otu84		0.36	0.30	Candidate division OP8
otu136		0.35		Candidate division OP8
otu82		0.32		Desulfarculaceae
otu134		0.32	0.30	vadinBA26
otu142		0.31		LCP-89
otu45			0.86	Napoli-4B-65
otu27			0.82	MSB-5B2
otu125			0.80	MSBL5
otu70			0.57	BHI80-139
otu107			0.50	Candidate division OP8
otu69			0.43	FW22
otu160			0.34	CCM11a
otu83			0.32	vadinBA26
otu177			0.31	TA06
otu22			0.31	SAR406 clade(Marine group A)
otu133			0.30	Sh765B-AG-111
otu142			0.29	LCP-89
otu329			0.29	MSBL5
Tot	45.04	45.19	45.28	
nOTU	54	48	55	

Table S2. SIMPER analysis performed on bacterial subsurface OTUs relative abundances. Here, only OTUs that show up to 45% of the observed dissimilarity are shown. A1, A2 and A3 are constituted by sequences from both 110 and 410 cm layers.

(previous page)

a

OTU	A0 (%)	A1 (%)	A2 (%)	Taxa
otu10	3.70	0.49	0.39	OM1 clade
otu51	0.98		0.14	OM1 clade
otu170	0.79	0.84	0.87	SAR406 clade(Marine group A)
otu35	0.77	0.62	0.66	Flavobacteriaceae
otu57	0.76	0.20	0.26	Pir4 lineage
otu101	0.74	0.81	0.82	SAR406 clade(Marine group A)
otu46	0.69		0.20	S085
otu187	0.69	0.74	0.74	JTB255 marine benthic group
otu112	0.65	0.73	0.72	Flavobacteriaceae
otu30	0.65	0.61	0.62	JTB255 marine benthic group
otu129	0.63	0.68	0.69	SEEP-SRB1
otu283	0.55			Pseudomonas
otu95	0.55	0.44	0.40	JTB255 marine benthic group
otu93	0.53	0.31	0.26	Flammeovirgaceae
otu59	0.51	0.19	0.24	Acidimicrobiaceae
otu173	0.48	0.52	0.53	Anaerolineaceae
otu86	0.47	0.70	0.47	JTB255 marine benthic group
otu39	0.47			Rhodospirillaceae
otu66	0.47			Nitrosomonas
otu231	0.45			Rubritalea
otu165	0.44		0.20	Sh765B-TzT-29
otu230	0.43			OM1 clade
otu150	0.43	0.47	0.47	Anaerolineaceae
otu34	0.42			Rhodobium
otu38	0.42	0.32	0.27	Pseudahrensia
otu211	0.42			Rhodobacteraceae
otu192	0.41	0.42	0.37	JTB255 marine benthic group
otu180	0.39	0.41	0.42	Cryomorphaceae
otu543	0.39	0.43	0.43	Candidate division KB1
otu212	0.39			Pelagibius
otu286	0.39	0.42	0.43	BD2-2
otu49	0.37	0.19	0.21	OM1 clade
otu73	0.36			Rhodospirillaceae
otu408	0.36	0.39	0.40	Desulfarculaceae
otu224	0.35	0.38	0.38	VC2.1 Bac22
otu60	0.35	0.66	0.49	JTB255 marine benthic group
otu120	0.34	0.17	0.20	Halioglobus
otu199	0.33	0.36	0.37	Anaerolineaceae
otu470	0.33			Rhodobacteraceae
otu140	0.32	0.33	0.21	JTB255 marine benthic group
otu246	0.31	0.34	0.35	SEEP-SRB1
otu302	0.30	0.33	0.33	LCP-89
otu18	0.30	0.78	0.40	JTB23
otu377	0.28			Flammeovirgaceae
otu498	0.27	0.29	0.30	Desulfarculaceae
otu402	0.25	0.27	0.28	Candidate division OP8
otu213	0.25	0.26	0.21	JTB255 marine benthic group
otu28		0.81	0.66	JTB23
otu43		0.41	0.32	JTB255 marine benthic group
otu163		0.40	0.28	JTB255 marine benthic group
otu25		0.34	0.29	Rhodobium
otu385		0.32	0.18	JTB255 marine benthic group
otu183		0.31	0.18	JTB23
otu48		0.25	0.26	Candidate division JS1
otu131		0.25	0.25	Candidate division JS1

b

OTU	A0 (%)	A1 (%)	A2 (%)	Taxa
otu50		0.25	0.25	Desulfarculaceae
otu475		0.25	0.25	SEEP-SRB1
otu614		0.24	0.24	BD2-11 terrestrial group
otu490		0.22	0.23	Sphingobacteriales
otu794		0.22	0.22	Candidate division OP8
otu263		0.22	0.17	JTB23
otu235		0.22	0.17	Sh765B-TzT-29
otu274		0.22	0.16	JTB255 marine benthic group
otu104		0.22	0.15	Marinicella
otu315		0.21	0.20	Flavobacteriaceae
otu122		0.20	0.15	Acidimicrobiaceae
otu176		0.20	0.15	BD7-8 marine group
otu316		0.20	0.18	JTB255 marine benthic group
otu169		0.19		Xanthomonadales
otu262		0.19	0.18	Marinicella
otu510		0.19		Sh765B-TzT-29
otu266		0.19		JTB255 marine benthic group
otu128		0.19		JTB255 marine benthic group
otu97		0.19		OM1 clade
otu4		0.18	0.19	Candidate division JS1
otu620		0.18	0.19	Desulfobacteraceae
otu1018		0.18	0.18	BD2-2
otu26		0.18	0.19	Anaerolineaceae
otu544		0.18	0.18	Proteobacteria
otu572		0.18	0.18	Desulfobacula
otu256		0.18		SHA-43
otu182		0.18		Marinicella
otu135		0.18	0.23	Flavobacteriaceae
otu507		0.18	0.18	WCHB1-69
otu627		0.17	0.18	Anaerolineaceae
otu1346		0.17	0.18	Candidate division OP3
otu306		0.17		BD7-8 marine group
otu132		0.17	0.18	Ulvibacter
otu599		0.16	0.16	WCHB1-69
otu682		0.16	0.15	Marinicella
otu328		0.16		JTB255 marine benthic group
otu257			0.24	Persicirhabdus
otu336			0.24	BD7-8 marine group
otu6			0.23	Hyphomicrobiaceae
otu768			0.19	Rubritalea
otu261			0.17	Roseibacillus
otu380			0.17	Persicirhabdus
otu631			0.16	BD7-8 marine group
otu798			0.16	BD2-2
otu29			0.16	MSBL2
otu333			0.15	JTB255 marine benthic group
otu452			0.15	Desulfarculaceae
otu403			0.15	Flavobacteriaceae
otu533			0.15	Lutibacter
otu795			0.15	Dehalococcoidia
otu640			0.14	Flavobacteriaceae
otu1345			0.14	Candidate division OD1
otu493			0.14	Sva1033
Tot	25.13	25.13	25.08	
nOTU	47	77	88	

Table S3. SIMPER analysis performed on bacterial surface OTUs relative abundances. The values are obtained comparing A0, A1 and A2 with A3. Here, A2 and A3 are constituted by the union of A2 and A2m, and A3 and A3m, respectively. Here, only OTUs that show up to 25% of the observed dissimilarity are shown. A) 1st part of the table; 2) 2nd part of the table.

8. Bibliography

Alain K, Olagnon M, Desbruye D, Page A, Barbier G, Juniper SK, Querellou JI, Cambon-Bonavita MA, 2002. Phylogenetic characterization of the bacterial assemblage associated with mucous secretions of the hydrothermal vent polychaete *Paralvinella palmiformis*. FEMS Microbiology Ecology, 42: 463-476.

Anderson RE, Sogin ML, Baross JA, 2015. Biogeography and ecology of the rare and abundant microbial lineages in deep-sea hydrothermal vents. FEMS Microbiology Ecology, 91(1): 1-11.

Andrea K. Bartram AK, Lynch MDJ, Stearns JC, Moreno-Hagelsieb G, Neufeld JD, 2001. Generation of Multimillion-Sequence 16S rRNA Gene Libraries from Complex Microbial Communities by Assembling Paired-End Illumina Reads. Applied Environmental Microbiology, 77(11): 3846-3852.

Bach W, Banerjee NR, Dick HJB, Baker ET, 2002. Discovery of ancient and active hydrothermal systems along the ultra-slow spreading Southwest Indian Ridge 10°-16°E. Geochemistry Geophysics Geosystems, 3: 1525-2027.

Baker ET, Chen YJ, Morgan JP, 1996. The relationship between near-axis hydrothermal cooling and the spreading rate of mid-ocean ridges. Earth and Planetary Science Letters, 142(1-2): 137-145.

Baker ET, Edmonds HN, Michael PJ, Bach W, Dick HJB, Snow JE, Walker SL, Banerjee NR, Langmuir CH, 2004. Hydrothermal venting in magma deserts: The ultraslowspreading Gakkel and Southwest Indian Ridges. Geochemistry Geophysics Geosystems, 5: 1-29.

Boetius A, 2005. Lost City Life. Science, 307: 1420-1422.

Bolger AM, Lohse M, Usadel B, 2014. Trimmomatic: a flexible trimmer for Illumina sequence data. Bioinformatics, 30(15): 2114-2120.

Camacho C, Coulouris G, Avagyan V, Ma N, Papadopoulos J, Bealer K, Madden TL, 2009. BLAST+: architecture and applications. BMC Bioinformatics, 10: 421.

Cannat M, Fontaine F, Escartín J, 2010. Serpentinization and Associated Hydrogen and Methane Fluxes at Slow Spreading Ridges. Geopshysical Monograph Series, 188: 241-264.

Castelle CJ, Wrighton KC, Thomas BC, Hug LA, Brown TB, Wilkins MJ, Frischkorn KR, Susannah G. Tringe SG, Singh A, Markillie LM, Taylor RC, Williams KH, Banfield JF, 2015. Genomic Expansion of Domain Archaea Highlights Roles for Organisms from New Phyla in Anaerobic Carbon Cycling. Current Biology, 25: 690-701.

Charlou JL, Donval JP, Konn C, Ondréas H, Fouquet Y, Jean-Baptiste P, Fourré E, 2010. High Production and Fluxes of H2 and CH4 and Evidence of Abiotic Hydrocarbon Synthesis by Serpentinization in Ultramafic-Hosted Hydrothermal Systems on the Mid-Atlantic Ridge. Geophysical Monograph Series, 188: 265-296.

Corliss JB, Dymond J, Gordon LI, Edmond JM, Von Herzen RP, Ballard RD, Green K, Williams D, Bainbridge A, Crane K, Van Andel TH, 1979. Submarine thermal springs on the Galapagos Rift. Science, 203: 1073-1083.

Danovaro R, Snelgrove PVR, Tyler P, 2014. Challenging the paradigms of deep-sea ecology. Trends in Ecology & Evolution, 29(8): 465-475.

DeLong EF, 2004. Microbial Life Breathes Deep. Science, 306: 2198-2200.

Dhillon A, Teske A, Dillon J, Stahl DA, Sogin ML, 2003. Molecular Characterization of Sulfate-Reducing Bacteria in the Guaymas Basin. Applied and Environmental Microbiology, 69(5): 2765-2772.

Dick GJ, Anantharaman K, Baker BJ, Li M, Reed DC, Sheik CS, 2013. The microbiology of deep-sea hydrothermal vent plumes: ecological and biogeographic linkages to seafloor and water column habitats. Frontiers in Microbiology, 4: 124.

Dick HJB, Jian Lin J, Schouten H, 2003. An ultraslow-spreading class of ocean ridge. Nature, 426: 405-412.

Ding J, Ding ZW, Fu L, Lu YZ, Cheng SH, Zeng RJ, 2015. New primers for detecting and quantifying denitrifying anaerobic methane oxidation archaea in different ecological niches. Applied Microbiology and Biotechnology, 99: 9805-9812.

Dutkiewicz A, Dietmar Müller R, O'Callaghan S, Jónasson H, 2015. Census of seafloor sediments in the world's ocean. Geology, 43(9): 795-798.

Edmonds HN, 2010. Chemical Signatures from Hydrothermal Venting on Slow Spreading Ridges. Geophysical Monograph Series, 188: 27-42.

Eme L and Doolittle WF, 2015. Microbial Diversity: A Bonanza of Phyla. Current Biology, 25(6): 227-230.

Fruh-Green GL, Kelley DS, Bernasconi SM, Karson JA, Ludwig KA, Butterfield DA, Boschi C, Proskurowski G, 2003. 30,000 Years of Hydrothermal Activity at the Lost City Vent Field. Science, 301: 495.

Gagolewski M and Tartanus B, 2015. R package stringi: Character string processing facilities. http://stringi.rexamine.com/. doi:10.5281/zenodo.19071.

German CR and Seyfried WE, 2014. Hydrothermal Processes. Treatise on Geochemistry, Second Edition, 8: 191-233.

German CR, Baker ET, Mevel C, Tamaki K, 1998. Hydrothermal activity along the southwest Indian Ridge. Nature, 395: 490-493.

German CR, Bowen A, Coleman ML, Honig DL, Huber JA, Jakuba MV, Kinsey JC, Kurz MD, Leroy S, McDermott JM, Mercier de Lépinav B, Nakamura B, Seewald JS, Smith JL, Sylva SP, Van Dover CL, Whitcomb LL, Yoerger DR, 2010. Diverse styles of submarine venting on the ultraslow spreading Mid-Cayman Rise. PNAS, 32: 14020-14025.

German CR, Lin J, Parson LM, 2013. The Thermal Structure of the Oceanic Crust, Ridge-Spreading and Hydrothermal Circulation: How Well do we Understand their Inter-Connections? Mid-Ocean Ridges (eds C.R. German, J. Lin and L.M. Parson), American Geophysical Union, Washington, doi: 10.1029/148GM01.

Hallberg KB, Hedrich S, Johnson DB, 2011. *Acidiferrobacter thiooxydans*, gen. nov. sp. nov.; an acidophilic, thermo-tolerant, facultatively anaerobic iron- and sulfur-oxidizer of the family Ectothiorhodospiraceae. Extremophiles, 15(2): 271-279.

Harrison BK, Zhang H, Berelson W, Orphan VJ, 2009. Variations in archaeal and bacterial diversity associated with the sulfate-methane transition zone in continental margin sediments (Santa Barbara Basin, California). Applied and Environmental Microbiology 75, 1487-1499.

Herndl GJ and Reinthaler T, 2013. Microbial control of the dark end of the biological pump. Nature Geoscience, 6: 718-724.

Hovland M, Jensen S, Fichler C, 2012. Methane and minor oil macro-seep systems-Their complexity and environmental significance. Marine Geology, 332: 163-173.

Hugler M and Sievert SM, 2011. Beyond the Calvin Cycle: Autotrophic Carbon Fixation in the Ocean. Annual Review of Marine Science, 3: 261-289.

Jeffrey A. Hawkes JA, Rossel PE, Stubbins A, Butterfield D, Connelly DP, Achterberg EP, Koschinsky A, Chavagnac V, Hansen CT, Bach W, Dittmar T, 2015. Efficient removal of recalcitrant deep-ocean dissolved organic matter during hydrothermal circulation. Nature Geoscience, 8: 856–860.

Jørgensen B, 1982. Mineralization of organic matter in the sea bed-the role of sulphate reduction. Nature, 296: 643-645.

Jørgensen BB and Boetius A, 2007. Feast and famine-microbial life in the deep-sea bed. Nature, 5, 770-781.

Kadnikov VV, Mardanov AV, Beletsky AV, Shubenkova OV, Pogodaeva TV, Zemskaya TI, Ravin NV, Skryabin KG, 2012. Microbial community structure in methane hydrate-bearing sediments of freshwater Lake Baikal. FEMS Microbiology Ecology, 79: 348-358.

Kelley DS, Baross JA, Delaney JR, 2002. Volcanoes, Fluids, and Life at Mid-Ocean Ridge Spreading Centers. Annual Review of Earth and Planetary Sciences, 30: 385-491.

Kelley DS, Früh-Green GL, Karson JA, Ludwig KA, 2007. The Lost City Hydrothermal Field Revisited. Oceanography, 20(4): 90-99.

Kelley DS, Karson JA, Fr ü h-Green GL, Yoerger DR, Shank TM, Butterfield DA, Hayes JM, Schrenk MO, Olson EJ, Proskurowski G, Jakuba M, Bradley A, Larson B, Ludwig K, Glickson D, Buckman K, Bradley AS, Brazelton WJ, Roe K, Elend MJ, Delacour A, Bernasconi SM, Lilley MD, Baross JA, Summons RE, Sylva SP, 2005. A Serpentinite-Hosted Ecosystem: The Lost City Hydrothermal Field. Science, 307: 1428-1434.

Leibold MA, Holyoak M, Mouquet N, Amarasekare P, Chase JM, Hoopes MF, Holt RD, Shurin JB, Law R, Tilman D, Loreau M, Gonzalez A, 2004. The metacommunity concept: a framework for multi-scale community ecology. Ecology Letters, 7(7): 601-613.

Liang B, Wang LY, Mbadinga SM, Liu JF, Yang SZ, Gu JD, Mu BZ, 2015. Anaerolineaceae and Methanosaeta turned to be the dominant microorganisms in alkanes-dependent methanogenic culture after long-term of incubation. AMB Express, 5:37.

Ludwig W, Strunk O, Westram R, Richter L, Meier H, Yadhukumar, Buchner A, Lai T, Steppi S, Jobb G, Förster W, Brettske I, Gerber S, Ginhart AW, Gross O, Grumann S, Hermann S, Jost R, König A, Thomas Liss, Lüßmann R, May M, Nonhoff B, Reichel B, Strehlow R, Stamatakis A, Stuckmann N, Vilbig A, Lenke M, Ludwig T, Bode A, Schleifer KH, 2004. ARB: a software environment for sequence data. Nucleic Acids Research, 32(4): 1363-1371.

Mahé F, Rognes T, Quince C, de Vargas C, Dunthorn M, 2014. Swarm: robust and fast clustering method for amplicon-based studies. PeerJ 2:e593

Martin M, 2011. Cutadapt removes adapter sequences from high-throughput sequencing reads. EMBnet.net

McCollom TM and Shock EL, 1997. Geochemical constraints on chemolithoautotrophic metabolism by microorganisms in seafloor hydrothermal systems. Geochimica et Cosmochimica Acta, 61(20): 4375–4391.

McGlynn SE, Chadwick GL, Kempes CP, Orphan VJ, 2015. Single cell activity reveals direct electron transfer in methanotrophic consortia. Nature, 526: 531-535.

McMurdie PJ and Holmes S, 2014. Shiny-phyloseq: Web Application for Interactive Microbiome Analysis with Provenance Tracking. Bioinformatics (Oxford, England), 31(2): 282-283.

Meyer JL, Akerman NH, Proskurowski G, Huber JA, 2013. Microbiological characterization of post-eruption “snowblower” vents at Axial Seamount, Juan de Fuca Ridge. Frontiers in microbiology, 4:153.

Middelburg JJ, Meysman FJR. Burial at Sea, 2007. Science, 316: 1294-1295.

Muyzer G and Stams AJ, 2008. The ecology and biotechnology of sulphate-reducing bacteria. Nature Reviews Microbiology, 6: 441-454.

Nakagawa, Takai K, Inagaki F, Hirayama H, Nunoura T, Horikoshi K, Sako Y, 2005. Distribution, phylogenetic diversity and physiological characteristics of epsilon-Proteobacteria in a deep-sea hydrothermal field. Environmental Microbiology, 7(10): 1619-1632.

Natland JH and Dick HJB, 2001. Formation of the lower ocean crust and the crystallization of gabbroic cumulates at a very slowly spreading ridge. Journal of Volcanology and Geothermal Research, 110(3-4): 191-233.

Nekola JC and White PS, 1999. The distance decay of similarity in biogeography and ecology. Journal of Biogeography, 26(4): 867-878.

Nunoura T, Takaki Y, Kazama H, Hirai M, Ashi J, Imachi H, Takai K, 2012. Microbial Diversity in Deep-sea Methane Seep Sediments Presented by SSU rRNA Gene Tag Sequencing. Microbes and Environments, 27(4): 382-390.

Ogawa H, Amagai Y, Koike I, Kaiser K, Benner R, 2001. Production of Refractory Dissolved Organic Matter by Bacteria. Science, 292(5518): 917-920.

Oksanen J, Blanchet GF, Kindt R, Legendre P, O’Hara BR, 2010. vegan: Community Ecology Package.

Orcutt BN, Joye SB, Kleindienst S, Knittel K, Ramette A, Samarkin V, Treude T, Boetius A, 2010. Impact of natural oil and higher hydrocarbons on microbial diversity, distribution, and activity in Gulf of Mexico cold-seep sediments. Deep Sea Research Part II: Topical Studies in Oceanography, 57(21–23): 2008–2021.

Orcutt BN, Sylvan JB, Knab NJ, Edwards KJ, 2011. Microbial Ecology of the Dark Ocean above, at, and below the Seafloor. Microbiology and Molecular Biology Reviews, 75, 361-422.

Orphan VJ, Hinrichs KU, Ussler III W, Paull CK, Taylor LT, Sylva SP, Hayes JM, Delong EF, 2001. Comparative Analysis of Methane-Oxidizing Archaea and Sulfate- Reducing Bacteria in Anoxic Marine Sediments. Applied and Environmental Microbiology, 67(4), 1922-1934.

Paradis E, Claude J, Strimmer K, 2004. APE: analyses of phylogenetic and evolution in R language. Bioinformatics, 20: 289-290.

Paull CK, Jull AJT, Toolin LJ, Linick T, 1985. Stable isotope evidence for chemosynthesis in an abyssal seep community. Nature, 317: 709-711.

Peng X, Chen S, Zhou H, Zhang L, Wu Z, Li J, Li J, Xu H, 2011. Diversity of biogenic minerals in low-temperature Si-rich deposits from a newly discovered hydrothermal field on the ultraslow spreading Southwest Indian Ridge. Journal of Geophysical Research, 116 (G3).

Pruesse E, Peplies J, Glöckner FO, 2012. SINA: accurate high-throughput multiple sequence alignment of ribosomal RNA genes. Bioinformatics, 28: 1823-1829.

Quast C, Pruesse E, Yilmaz P, Gerken J, Schweer T, Yarza P, Peplies J, Glöckner FO, 2013. The SILVA ribosomal RNA gene database project: improved data processing and web-based tools. Nucleic Acids Research, 41 (D1): 590-596.

R Foundation for Statistical Computing, Vienna, Austria, 2012. R: A language and environment for statistical computing.

Rinke C, Schwientek P, Sczyrba A, Ivanova NN, Anderson IJ, Cheng JF, Darling A, Malfatti S, Swan BK, Gies EA, 2013. Insights into the phylogeny and coding potential of microbial dark matter. Nature, 499: 431–437.

Ruff SE, Biddle JF, Teske AP, Knittel K, Boetius A, Ramette A, 2015. Global dispersion and local diversification of the methane seep microbiome. Proceedings of the National Academy of Sciences, 112(13): 4015-4020.

Ruff SE, Probandt D, Zinkann AN, Iversen MH, Klaas C, Würzberg L, Krombholz N, Wolf-Gladrow D, Amann R, Knittel K, 2014. Indications for algae-degrading benthic microbial communities in deep-sea sediments along the Antarctic Polar Front. Deep Sea Research Part II: Topical Studies in Oceanography, 108: 6-16.

Schreiber L, Holler T, Knittel K, Meyerdierks A, Amann R, 2010. Identification of the dominant sulfate-reducing bacterial partner of anaerobic methanotrophs of the ANME-2 clade. Environmental Microbiology, 12(8): 2327-2340.

Schrenk MO, Brazelton WJ, Lang SQ, 2013. Serpentinization, Carbon, and Deep Life. Reviews in Mineralogy & Geochemistry, 75: 575-606.

Snow J and Edmonds H, 2007 Ultraslow-Spreading Ridges, Rapid Paradigm Changes. Oceanography, 20: 90-101.

Sogin ML, Morrison HG, Huber JA, Welch DM, Huse SM, Neal PR, Arrieta JM, Herndl GJ, 2006. Microbial diversity in the deep sea and the underexplored “rare biosphere”. Proceedings of the National Academy of Sciences, 103(32): 12115-12120.

Sohn RA, Willis C, Humphris S, Shank TM, Singh H, Edmonds HN, Kunz C, Hedman U, Helmke E, Jakuba M, Liljebladh B, Linder J, Murphy C, Nakamura K, Sato T, Schlindwein V, Stranne C, Tausenfreund M, Upchurch L, Winsor P, Jakobsson M, Soule A, 2008. Explosive volcanism on the ultraslow-spreading Gakkel ridge, Arctic Ocean. Nature, 453: 1236-1238.

Stamatakis A, 2014. RAxML Version 8: A tool for Phylogenetic Analysis and Post-Analysis of Large Phylogenies. Bioinformatics, 30 (9): 1312-1313.

Standish JJ and Sims KWW, 2010. Young off-axis volcanism along the ultraslow-spreading Southwest Indian Ridge. Nature Geoscience, 3: 286-292.

Takai K, Gamo T, Tsunogai U, Nakayama N, Hirayama H, Nealson KH, Horikoshi K, 2004. Geochemical and microbiological evidence for a hydrogen-based, hyperthermophilic subsurface lithoautotrophic microbial ecosystem (HyperSLiME) beneath an active deep-sea hydrothermal field. Extremophiles, 8(4): 269-282.

Takano Y, Chikaraishi Y, Ogawa NO, Nomaki H, Morono Y, Inagaki F, Kitazato H, Hinrichs KU, Ohkouchi NO, 2010. Sedimentary membrane lipids recycled by deep-sea benthic archaea. Nature Geoscience, 3: 858-861.

Tao C, Lin J, Guo S, Chen YJ, Wu G, Han X, German CR, Yoerger DR, Zhou N, Li H, Su X, Zhu J, 2012. First active hydrothermal vents on an ultraslow-spreading center: Southwest Indian Ridge. Geology, 40: 47-50.

Tao CH, Li HM, Huang W, Han XQ, Wu GH; Su X, Zhou N, Lin J, He YH, Zhou JP, 2011. Mineralogical and geochemical features of sulfide chimneys from the 49°39′E hydrothermal field on the Southwest Indian Ridge and their geological inferences. Chinese Science Bulletin, 56: 2829-2838.

Tebbe CC and Vahjen W, 1993. Interference of humic acids and DNA extracted directly from soil in detection and transformation of recombinant DNA from bacteria and a yeast. Applied Environmental Microbiology, 59(8): 2657-2665.

Tunnicliffe V, 1988. Biogeography and evolution of hydrothermal vent fauna in the eastern Pacific Ocean. Proceedings of the Royal Society of London, 66: 233-347.

Tyler PA, German CR, Ramirez-Llodra E, Van Dover CL, 2003. Understanding the biogeography of chemosynthetic ecosystems - Comprendre la biogéographie des écosystèmes chémosynthétiques. Oceanologica Acta, 25: 227-241.

Van Dover CL, German CR, Speer KG, Parson LM, Vrijenhoek RC, 2002. Evolution and Biogeography of Deep-Sea Vent and Seep Invertebrates. Science, 295 (5558): 1253-1257.

Vannelli T, Logan M, Arciero DM, Hooper AB, 1990. Degradation of Halogenated Aliphatic Compounds By the Ammonia-Oxidizing Bacterium *Nitrosomonas europaea*. Applied and Environmental Microbiology, 56:1169-1171.

Walker CB, De La Torre JR, Klotz MG, Urakawa H, Pinel N, Arp DJ, Brochier-Armanet C, Chain PSG, Chan PP, Gollabgir A, Hemp J, Hügler M, Karr EA, Könneke M, Shin M, Lawton TJ, Lowe T, Martens-Habbena W, Sayavedra-Soto LA, Lang D, Sievert SM, Rosenzweig AC, Manning G, Stahl DA, 2010. *Nitrosopumilus maritimus* genome reveals unique mechanisms for nitrification and autotrophy in globally distributed marine crenarchaea. Proceedings of the National Academy of Sciences, 107(19): 8818-8823.

Webster G, Parkes RJ, Fry JC, Weigthman AJ, 2004. Widespread occurrence of a novel division of bacteria identified by 16S rRNA gene sequences originally found in deep marine sediments. Applied and Environmental Microbiology, 70: 5708-5713.

Whitman WB, Coleman DC, Wiebe WJ, 1998. Prokaryotes: The unseen majority. Proceedings of the National Academy of Sciences, 95: 6578-6583.

Wickham H, 2009. ggplot2: elegant graphics for data analysis. Springer New York.

Wickham H, 2011. The Split-Apply-Combine Strategy for Data Analysis. Journal of Statistical Software, 40(1): 1-29.

Xie W, Zhang C, Zhou X, Wang P, 2014. Salinity-dominated change in community structure and ecological function of Archaea from the lower Pearl River to coastal South China Sea. Applied Microbiology and Biotechnology, 98(18): 7971-7982.

Zhang J, Kobert K, Flouri T, Stamatakis A, 2013. PEAR: a fast and accurate Illumina Paired-End reAd mergeR. Bioinformatics, 30(5): 614-620.

Zinger L Boetius A, Ramette A, 2014. Bacterial taxa-area and distance-decay relationships in marine environments. Molecular Ecology, 23(4): 954-964.

Zinger L, Amaral-Zettler LA, Fuhrman JA, Horner-Devine MC, Huse SM, Welch BDM, Martiny JBH, Sogin M, Boetius A, Ramette A, 2011. Global Patterns of Bacterial Beta-Diversity in Seafloor and Seawater Ecosystems. PLoS ONE, 6(9), e24570.